**ADDIS ABABA UNIVERSITY**

**ADDIS ABABA INSTITUTE OF TECHNOLOGY**

**SCHOOL OF CIVIL AND ENVIRONMENTAL ENGINEERING**


# Blast-Earthquake Scenarios Comparative Response Analysis of Multi-Story Reinforced Frame Buildings

**A Thesis in Structural Engineering**

By Awol Garito

August 2020

Addis Ababa

A Thesis

Submitted in Partial Fulfillment of the Requirements for the Degree of Master of Science

The undersigned have examined the thesis entitled '**Blast-Earthquake Scenarios comparative response analysis of multi-story reinforced frame buildings'** presented by **Awol Garito**, a candidate for the degree of **Master of Science** and hereby certify that it is worthy of acceptance.

| | | |
|---|---|---|
| Dr. Shifferaw Taye | _____ | _____ |
| Advisor | Signature | Date |
| Dr.-Ing. Adil Zekaria | _____ | _____ |
| Internal Examiner | Signature | Date |
| Dr. Esayas G/Yohannes | _____ | _____ |
| External Examiner | Signature | Date |
| _____ | _____ | _____ |
| Chair person | Signature | Date |

## UNDERTAKING

I certify that research work titled “Blast-Earthquake Scenarios comparative response analysis of multi-story reinforced frame buildings” is my own work. The work has not been presented elsewhere for assessment. Where material has been used from other sources it has been properly acknowledged / referred.

Awol Garito

## ABSTRACT

This thesis deals with the comparative structural modelling and analysis of different multi-story RC frame structures for sub surface blast loads and earth quake loads. The thesis discusses the dynamic responses of two RC frame structure with different number of bays and stories that happen to blasting vibration waves generated using amount of explosion at different stand of distance and earth quake vibration waves characterized by the elastic design spectrum (Type 1 and 2) and different ground types of ES EN1998-1, 2015 scaled to different peak ground acceleration and 5% damping.

The RC frame structure was analyzed for sub surface blast loads using linear direct integration time history analysis method for its dynamic responses. It has been found that explosion source distance is the main influencing factor in blast loads, the larger the explosion distance the smaller is change rate of floor displacement irrespective of the height of the structure. It has also been found that a larger number of bays results in weaker blasting vibration responses.

Responses of the RC frame structure for earth quake loads has been found using elastic response spectrum analysis. The results are compared with the responses of the structure for the blast loads and it has been found that the global responses of considered RC frame structures subjected to blast loads at nearer standoff distance and earth quake loads of 0.2g is almost comparable but at farther stands of distance, the global responses of RC frame structure for the blast loads are insignificant.

## ACKNOWLEDGMENTS

Firstly, I thank Allah the merciful for that I am enable to fulfil this work. Next my deepest gratitude and appreciation goes to my adviser Dr. Shifferaw Taye for proposing me such an interesting area of study and for his guidance and supervision since the beginning of the study.

Then I wish to thank my sponsor (ERA) Ethiopian road authority for giving me the chance.

Finally, I would like to express my deepest gratitude to my parents; for their patience and care throughout the duration of study, and to my friends who contributed to this thesis in one way or another.

## TABLE OF CONTENTS

## LIST OF TABLES

## LIST OF FIGURES

# CHAPTER 1 INTRODUCTION

## 1.1 Back ground

Blast loads have come in to attentions in recent years due to the great number of accidental or intentional events that affected important structures all over the world, clearly indicating that the issue is relevant for purposes of structural design and reliability analysis [12]. Disasters such as the bombings of the U.S. embassies in Nairobi, Kenya and Dares Salaam, Tanzania in 1998, the Khobar Towers military barracks in Dhahran, Saudi Arabia in 1996, the Murrah Federal Building in Oklahoma City in 1995, and the World Trade Center in New York in 1993 are the most notable recent examples. In consequence, extensive research activities in the field of blast loads have taken place in the last decades and there has been heightened interest among building owners and government entities in evaluating the progressive collapse potential of existing buildings, and in designing new buildings to resist this type of collapse [11].

The energy of explosion is used in the fields of civil/structural engineering, mining, agriculture and forestry. Explosions in underground installations arise from explosives, plant failure or from external rockets/missiles detonating at great depths. Nuclear explosions are adopted for finding underground resources. In mining, explosions have been adopted for tunneling, coal mining and canal works. In agriculture and forestry, explosive methods are used to sink piles for tree planting, stump extraction and irrigation system construction [1].

Much effort has been devoted to the study of underground explosions because they present an actual risk. According to the 1999 Landmine Monitor report from the international Committee to Ban Landmines, estimates on the number of buried landmines worldwide range from 60 to 110 million. Protective equipment, either for personnel or vehicles, must be designed to mitigate the effect of a landmine blast. As a result, there is a need for modelling and understanding the interaction of mine blast products with structures and the resulting loading and damage mechanisms inflicted by explosive blast and impact. This understanding is required both for damage assessment and protective hardening of both wheeled and tracked vehicles [12].

By the other side, reinforced concrete structures are used for essential installations protected against the effects of conventional weapons. The physical processes that govern the response of the structure are very complex, involving dynamic interactions among the explosive, the soil and the structure. Major phenomena include the formation of the crater or camouflet by the explosion; the propagation of the shock wave and elastic–plastic wave in the soil; and the interaction between soil and the structure. The high intensity, short term loading imparted by the explosion is enormously complex and can be significantly affected by a number of parameters including the size, shape, type, detonation point and depth of burial of the explosive and the type, density and water content of the soil [1,16].

The potential threat of an explosion is random in nature. Therefore, the analysis becomes complex and it is necessary to identify the influence of each factor in relation to the most credible event when assessing the vulnerability of structures [13]. Difficulties that arise with the complexity of the problem consequences from blast loading which involves time dependent finite deformations, high strain rates, and non - linear inelastic material behavior, have motivated various assumptions and approximations to simplify the load as well as structural models. These models span the full range of sophistication from single degree of freedom systems to more complex computer based applications [11].

## 1.2 Objectives of the thesis

The main objective is to study the effects of sub surface blast on RC frame structure and to investigate blast seismic effects on RC frame structure relative to seismic effects of earth quake.

Specific objectives

- To model and analyze deferent multistory RC framed structure for deferent sub surface blast loads under deferent parameters.
- To investigate the dynamic response of multistory RC framed structures subjected to subsurface blast loading and earth quake loading.
- To look into available procedure for sub surface blast analysis on framed structures.
- To establish the relationship between sub surface blast loads and seismic loads.

## 1.3 Contents and organizations of the thesis

The thesis is divided into five chapters:

- General introduction to the blast loading and its effects on building is described in chapter one.
- Chapter two explains the explosions definition, blast wave phenomena, blast induced ground vibrations and empirical formulas available in different literature for generating blast induced ground vibration motion, and the relation between seismic waves generated by blast and earth quake. Furthermore, blast load prediction methods are also reviewed in this chapter.
- Chapter three deals briefly the blast analysis methods including SDOF approximation and computer based finite element analysis.
- A numerical study on reinforced concrete structure subjected to blast loading and earth quake loading is presented in chapter four. A preliminary design and analysis procedures for both blast and earth quake loads are briefly covered in this chapter. Analysis results are presented and discussed as well.
- Finally, conclusions drawn for this thesis work and the recommendations for the future work are presented in chapter five.

# CHAPTER 2 BLAST LOADING AND EARTH QUAKE LOADING

## 2.1 Introduction

An explosion is a rapid and sudden release of stored potential energy characterized by a bright flash and an audible blast. Part of the energy is released as thermal radiation (flash); and part is coupled into the air as air blast and into the soil (ground) as ground shock, both as radially expanding shock waves.

Blast loading is unlike other types of severe loads caused by extreme events such as earthquake or high wind. These types of loads generate damage that is limited to a very few structural response mechanisms, and they are applied "globally" such that the entire structural system works to resist the load. Explosive blast activates many structural response mechanisms because of its extreme spatial and time variations in magnitude and time of application (duration) [11].

## 2.2 Blast loading and earth quake loading

Two of the most destructive events that a building structure could experience are earthquake and blast. In designing a building structure to resist the forces induced by an earthquake, both the local response at the element level and the global response are considered. However, despite the similarities between seismic excitation and blast loading, the global response of buildings to blast loading is usually not considered as being critical. The response of building structures to blast loading is traditionally assessed by individual analysis of its critical members. While this type of assessment can be conservative, it does not provide an estimate of the global response of the building, particularly of the deformations in the lateral load resisting system, which can at times be critical. On the other hand, the global deformations, such as inter- story drifts, have been traditionally considered as being among the most important response parameters of the building structures subjected to earthquakes [14].

### 2.2.1 Blast loading

Blast loads on structures can be divided into two main groups based on the confinement of the explosive charge (unconfined and confined explosions) and can be subdivided based on the blast loading produced within the donor structure or acting on acceptor structures [10].

**a) Unconfined Explosion**

- Free Air Burst Explosion

An explosion, which occurs in free air, produces an initial output whose shock wave propagates away from the center of the detonation, striking the protective structure without intermediate amplification of its wave.

- Air Burst Explosion

An explosion which is located at a distance from and above the protective structure so that the ground reflections of the initial wave occur prior to the arrival of the blast wave at the protective structure [1].

- Surface Burst Explosion

A surface burst explosion will occur when the detonation is located close to or on the ground so that the initial shock is amplified at the point of detonation due to the ground reflections [1].

**b) Confined Explosion**

- Fully Vented Explosion

A fully vented explosion will be produced within or immediately adjacent to a barrier or cubicle type structure with one or more surfaces open to the atmosphere.

- Partially Confined Explosion

A partially confined explosion will be produced within a barrier or cubicle type structure with limited size openings and/or frangible surfaces.

- Fully Confined Explosions

Full confinement of an explosion is associated with either total or near total containment of the explosion by a barrier structure. Internal blast loads will consist of unvented shock loads and very long duration gas pressures which are a function of the degree of containment.

### 2.2.2 Explosions and Earthquakes as a Seismic Source

The term "seismic source" is a comprehensive name for all events or, more generally, for any radiator of seismic waves. A seismic source can be described by its strength and its spatial and temporal characteristics, i. e., by parameters such as source dimension, geometry and time function of the radiation. The spatial as well as the temporal dimensions of an explosion are smaller than those of an earthquake of comparable strength. Moreover, an explosion is almost truly symmetric, whereas a great many earthquake source are highly unsymmetrical. The natural earthquakes especially those of large magnitude- always exhibit certain extension, both in time and space. Often the rupture starts at one end of the fault and propagates with a velocity of around 3 km/sec along the fault to its opposite end. This entails that, a comprehensive spectrum of seismic waves is generated and those records are obtained on both short- period and long- period seismographs. Time duration of oscillation is influenced by many factors. In an isotropic unbounded homogeneous medium mainly the characteristic dimensions of the source influence the time duration [24].

Knowledge of the properties of explosion-generated seismic waves is largely empirical based on the analysis of countless seismograms produced by explosions covering a tremendous range of yields and fired under a wide variety of conditions. Attempts to understand this large body of data have led to theoretical developments concerning the processes of wave formation and wave propagation that are the foundation of this branch of seismology. Many aspects of this theory are well-developed, because of the complex nature of the materials of which the earth is composed and the complex structure of the medium through which the waves must propagate to the seismograph, the interpretation of particular observations is often difficult. In particular, the seismologist is called upon to isolate the effects of a number of variable parameters that are part of the circumstances surrounding any test explosion [21].

The ground motion recorded at a given recording site corresponds to the superposition in time of seismic waves which have travelled from the energy source to the receiver along a great number of travel paths. Consequently, the amplitude of a specific wave type recorded at an individual station is a complex function of variables related to;

1) The source region,

2) The transmission path, and

3) The recording site.

Source variables include the yield of the device, the depth of burial, the nature of the emplacement hole, and physical parameters (rock type, elastic properties, moisture content, propagation velocity, etc.) of the source and near-source media. Transmission path variables include the physical parameters of each individual transmission path between the source and receiver, the source to receiver distance, the geometrical travel path, and the propagating elastic wave type. Recording site variables include the physical parameters (thickness, elastic properties, rock type, etc.) of the near.-surface materials, geophone-earth coupling, and instrument response characteristics [22].

There are three principal sources of seismic signals from underground nuclear explosions. The first, and most significant, is the explosion itself. The second is chimney or mound collapse which involves the fall of millions of tons of rock. The third appears to be a consequence of explosion-produced strain changes in the neighboring kilometers of rock which are released as a series of aftershocks. The seismic signals that are emitted downward from the explosion itself (not from chimney collapse or aftershocks) are those which are recorded as the first arrivals at epicenter distances of several hundred to a few thousand kilometers. At these distances there appears to be no noticeable differences between the signals (used to determine magnitude) from contained and cratering events, all other conditions such as yield and geology being equal.

There are many differences between earthquakes and explosions; those of concern in this thesis are the differences in relative energy content of the various

types of elastic waves generated by these two types of events. Two types of elastic waves may be propagated within an isotropic, homogeneous elastic solid body: compressional or P waves and shear or S waves. If a finite, three-dimensional wave source (e.g., an explosion) is perfectly spherical, only P waves are generated; if not, both P and S waves are produced. Observations near underground nuclear explosions indicate that mostly P and relatively few S waves are generally produced, implying that such explosions tend to be spherical. In contrast, earthquakes generally produce strong S waves as well as P waves, indicating the geometry of earthquake sources is not spherical. Of course, it must be remembered that the earth is not homogeneous, and that partial conversion of P waves to S waves and vice versa is associated with reflections and refractions of elastic waves by various non-homogeneities. In the case of one important inhomogeneity the free surface of the earth, the impinging P and S waves also interact with the surface in such a manner that Rayleigh or R waves and (under special conditions of layering), Love or L waves are generated. Unlike P and S waves which travel within an elastic body (hence the term body waves), R and L wave motions are concentrated at and near the surface so are called surface waves. The principal seismic method of distinguishing earthquakes from explosions at distances of thousands of kilometers is that of comparing the surface (R)-wave magnitude with the body (P)-wave magnitude. It is apparent that earthquakes tend to produce significantly stronger R-wave signals than do explosions with the same body-wave magnitude. This may be a consequence of explosions producing relatively weak S waves and hence weak R waves. Nuclear explosions tend to produce much weaker S and R waves than do earthquakes of comparable body wave magnitude. As a consequence, the seismic wave energy associated with an earthquake of a given body wave magnitude is less than that of an explosion of equal magnitude [23].

In the work by (Sayed A. Dahy and Gaber H. Hassib 2010), a trial was made to discriminate between quarry blasts and regional micro earthquakes using the records of Aswan seismic network and these trials are spectral analysis and spectral amplitude ratio methods. Spectral analysis method will be considered through a rather individual viewpoint, treating the whole subject as the

accumulation of largely convolution effects in the frequency domain. The conventional approach to spectral analysis, whereas by a time series is decomposed into its Fourier components, was originally based on the computation of the auto- correlation of a time series whose spectrum was desired. The spectral analyses of 4 events were recorded by two seismic stations from Aswan network are shown in Figs 2.1 and 2.2. For the spectral analysis a time-window length was chosen individually for every seismogram. The amplitude velocity spectra were calculated from vertical component seismograms at the last two seismic stations. It is obvious that, the earthquake spectra are peaked in the range from 8 to 18 (Hz) band, with little energy below 6 Hz, whereas the explosion spectra have flatter spectra from about 3 to 16 Hz. This difference in the spectra may be caused the earthquakes occurring at greater depths than the quarry blasts, differences in the near source media, or source mechanism effects in the earthquake spectra.

The quarry blasts spectra exhibit marked scalloping or modulation patterns not observed in the earthquake spectra. The modulation patterns are identical in spectra of all phases, indicating that they are caused by multiple- shot sequences or ripple firing. Also, Figs 2.1 and 2.2 show that earthquake waves contain slightly lower frequency than the waves generated by blasts, i.e., they produce seismic waves of different frequency content. Concerning different types of waves, P- wave is stronger, relative to other phases, for quarry blasts than for earthquakes and the amplitude ratio of log (As/Ap) generated by blasts is not greater than that of earthquakes indicating that the seismic wave caused by quarry blast can cause considerable damage to the target structure [24].

When estimates began to be made, in the early 1990s, of the numbers of chemical explosions set off routinely in industrialized countries, there was concern that the seismic signals from such explosions would be so numerous. The reasoning behind such pessimism was that the United States, Russia, China, and numerous non-nuclear-weapon states such as Australia, Canada, Kazakhstan, and countries of South America use a total of about 5 mt of chemical explosive per year. This overall total is distributed across numerous blasts of total charge size ranging

above 1 kt (on the order of a few hundred per year), between 100 and 1000 tons (thousands per year), and between 10 and 100 tons (many thousands per year).

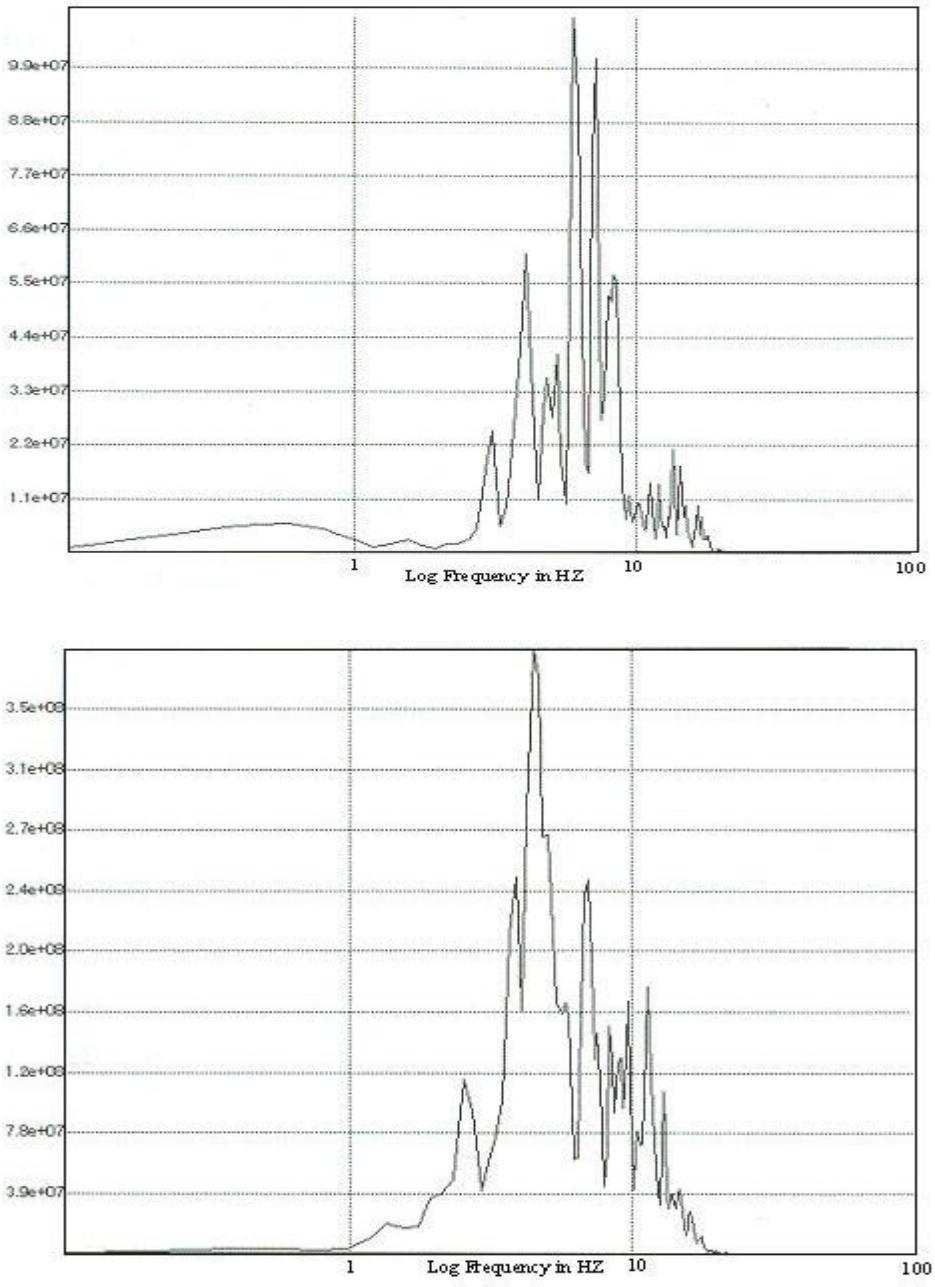


**Figure 2.1:The velocity amplitude spectra of two micro earthquakes with magnitudes 2.6 and 2.3 respectively [24].**

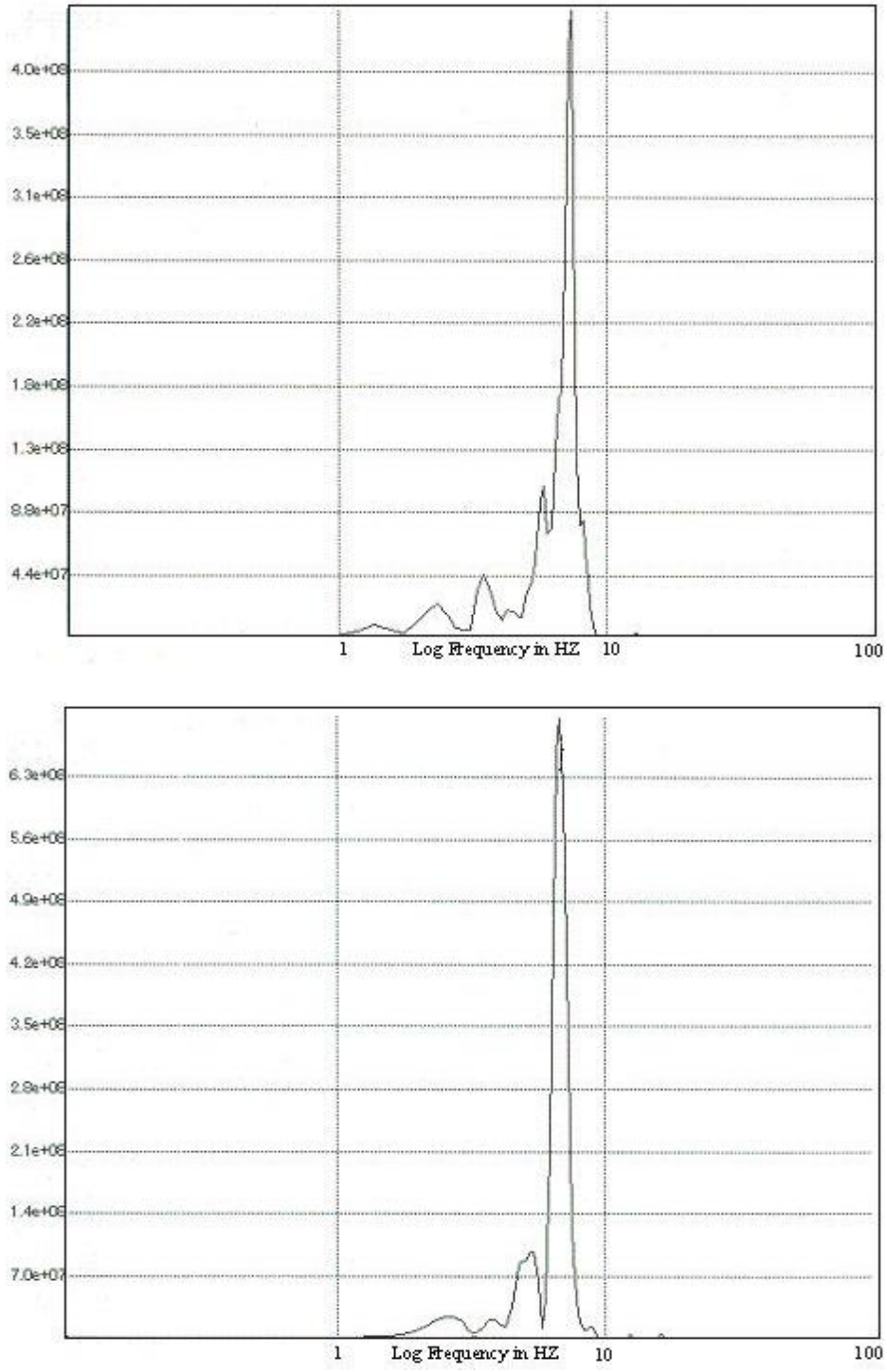


**Figure 2.2: The velocity amplitude spectra of two quarry blasts with magnitudes 2.6 and 2.3 respectively [24].**

If these charge sizes were interpreted via equation given in different literatures, then one would expect chemical explosions to generate hundreds of events each year with magnitude greater than 4.5, thousands of events per year in the

magnitude range 3.5 to 4.5, and several events per hour in the range 3 to 3.5 (a magnitude range that includes the source strength predicted for around 5 kt [26].

## 2.3 Blast wave phenomena

The violent release of energy from a detonation converts the explosive material into a very high pressure gas at very high temperatures. A pressure front associated with the high pressure gas propagates radially into the surrounding atmosphere as a strong shock wave, driven and supported by the hot gases. The shock front, termed the blast wave, is characterized by an almost instantaneous rise from ambient pressure to a peak incident pressure $P_{so}$ (Fig 2.3).

This pressure increase or shock front travels radially from the burst point with a diminishing shock velocity which is always in excess of the sonic velocity of the medium. Gas molecules behind the front move at lower flow velocities, termed particle velocities. These latter particle velocities are associated with the dynamic pressures or the pressures formed by the winds produced by the passage of the shock front.

As the shock front expands into increasingly larger volumes of the medium, the peak incident pressures at the fronts decrease and the durations of the pressures increase [10].

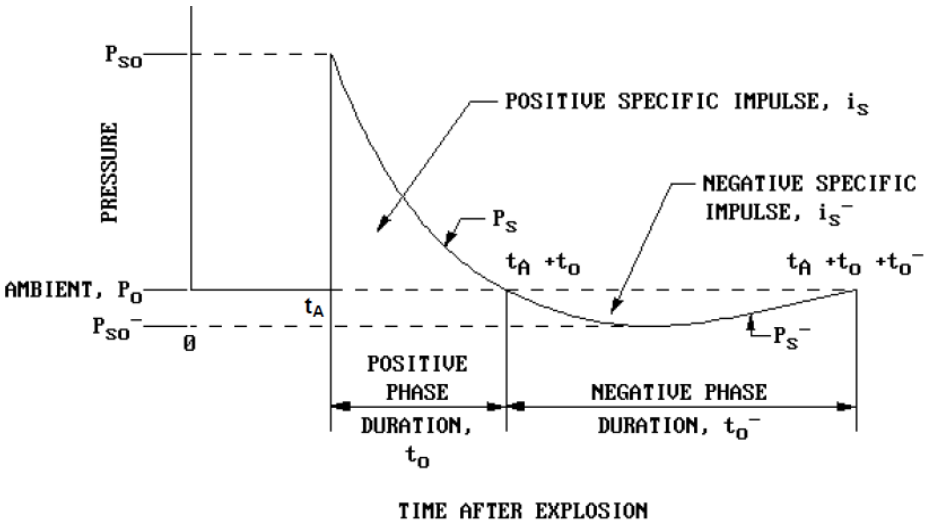


**Figure 2.3: Free-Field Pressure-Time variation [10].**

The shock front arrives at a given location at time $t_A$ and, after the rise to the peak value, $P_{so}$ the incident pressure decays to the ambient value in time to which is the positive phase duration. This is followed by a negative phase with a duration $t_0^-$ that is usually much longer than the positive phase and characterized by a negative pressure (below ambient pressure) having a maximum value of $P_{S0}^-$ as well as a reversal of the particle flow. The negative phase is usually less important in a design than is the positive phase, and its amplitude $P_S^-$ must, in all cases, be less than ambient atmosphere pressure $P_0$. The incident impulse density associated with the blast wave is the integrated area under the pressure-time curve and is denoted as $i_S$ for the positive phase and $i_S^-$ for the negative phase.

### 2.3.1 Phenomena of sub surface blast and blast wave

When a buried charge explodes, the resulting energy transmitted in the air depends on the conditions of the burial: if the charge is buried too deeply, there will not be enough energy for the shock wave to reach the surface. The detonation products remain in the soil, and the explosion is called a camouflet [14].

The pressure of the explosive gases immediately after detonation causes the soil adjacent to the charge surface to be crushed and eventually to change into a liquid state. The zone is highly deformed. The size of the deformation changes as the distance from the centre of the source of detonation increases. Due to high tensile stresses, cracks/fissures are developed. From the source, the soil which looks like a brittle one is surrounded by a chamber of three zones in the order: crushing zone, rupture zone and elastic zone. Various waves and their reflections occur. In some cases, swelling occurs [1].

The buried explosion generates three types of waves in the soil: compression, shear and Rayleigh waves. The intensity of the induced soil displacement decreases as they propagate. While the compressive and shear waves propagate in a spherical manner, the expansion of the Rayleigh waves is cylindrical.

For the three waves, the rate of decay depends on the soil properties, in particular the density (which can amplify the shock intensity up to two orders of magnitude

and the water content. A saturated soil has a larger stiffness and strength, and the shock propagates faster and more easily [14].

A buried explosion involves three main stages: first, the detonation of the explosive and the early interaction between the explosive and the soil; second, the gas expansion and the first ejecta from the soil; finally, the momentum transferred from the whole soil initially located above the explosives broken in ejecta. These phenomena are highlighted in Fig 2.4 [1, 15].

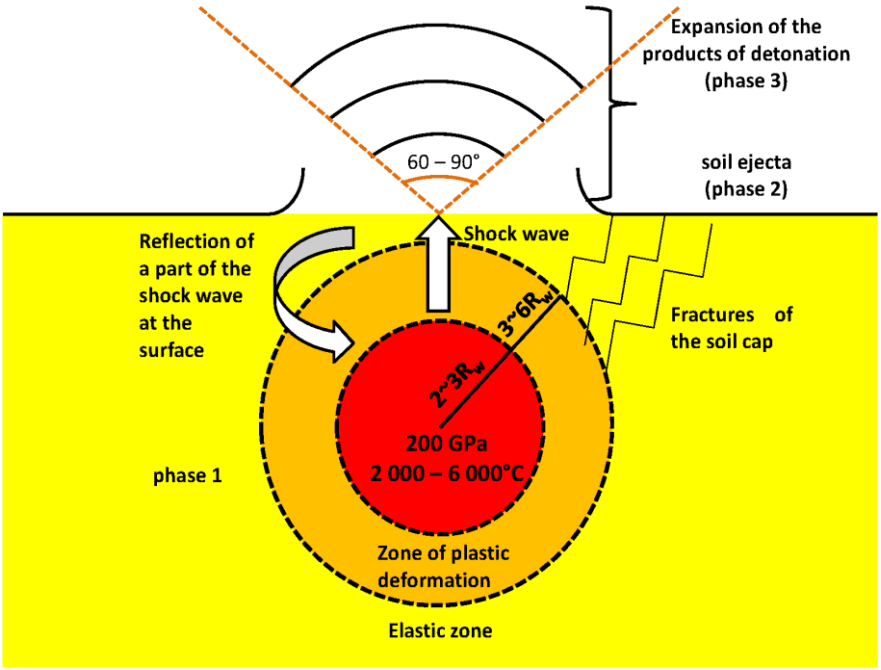


**Figure 2.4: The three stages that take place during a buried explosion [15].**

- First stage: detonation and early interaction between the explosive and the soil

At detonation, the solid explosive is transformed into detonation gases at high pressure (around 200 GPa) and high temperature (between 2,000 and 6,000◦C). In the soil, three areas shown in Fig 2.4 can be observed depending on the distance from the detonation point. Very close and along a distance of two or three explosive radii, the soil is so crushed with a so high temperature and pressure that the propagation of the shock wave can be considered independent on the medium properties. A plastic zone is extended from three to six radii of the explosive

where the shock wave has provoked irreversible soil compression. The density and the volume fraction of the air have notably changed and can be two key parameters to determine the size of the zone.

Outside these two zones, the soil can be considered as elastic since the explosion has caused mostly reversible changes. The early interaction between the explosive and the soil is the most important stage because it determines the quantity of energy which will be available to generate the impulse on a target located above the soil. The depth of burial of the explosive, the water content of the soil, and its physical properties are thought to have the largest.

- Second stage: Gas expansion and early ejecta

After the early interaction between the explosive and the soil, the shock wave propagates up to the surface. There, a large difference of impedance exists between the soil and the air. The impedance corresponds to the product of the density times the sound speed of the medium. As a consequence, a part of the shock wave is transmitted in the air whereas the other part is reflected in the soil as a tensile wave. When propagating in the air, the shock wave drives a little part of the soil from the surface. They are the early ejecta.

- Third stage: Transfer of momentum from soil ejecta

The propagation of the shock wave weakens the soil which is now fractured. The detonation products can find a way to the surface through the soil fractures and drive finally all the soil above the explosive upward at speeds of hundreds of meters per second. The soil projections have kinetic energy which contributes to the impulse. The set of soil ejecta have a conical geometrical form with an angle from 60 to $90^0$. This angle decreases as the depth of burial and the soil density increase. These three steps occur in a few milliseconds.

## 2.4 Prediction of blast pressure

The following methods are available for prediction of blast effects on building structures: [6].

- Empirical (or analytical) methods
- Semi-empirical methods
- Numerical (or first-principle) methods.

Empirical methods are essentially correlations with experimental data. Most of these approaches are limited by the extent of the underlying experimental database. The accuracy of all empirical equations diminishes as the explosive event becomes increasingly near field. Some of empirical equations that are currently available for blast load predictions are, TM 5-1300 (US Department of the Army, 1990), UFC (Unified Facility Criteria)

Semi-empirical methods are based on simplified models of physical phenomena. They attempt to model the underlying important physical processes in a simplified way. These methods rely on extensive data and case study. Their predictive accuracy is generally better than that provided by the empirical methods.

Numerical (or first-principle) methods are based on mathematical equations that describe the basic laws of physics governing a problem. These principles include conservation of mass, momentum, and energy. In addition, the physical behaviour of materials is described by constitutive relationships. These models are commonly termed computational fluid dynamics (CFD) models.

## 2.5 Sub-surface blast induced ground vibration motion

Explosion-generated ground motions can be described by three perpendicular components: longitudinal, vertical and transverse (Fig 2.5). The longitudinal vibration is usually oriented along the explosion radius while the other two components are vertical and transverse to the radial direction. Generally, blasting induced ground motion is measured in particle vibration time history. The important vibration parameters are peak amplitude, principal frequency and duration. Peak particle velocity (PPV) and principal frequency (PF) are the most commonly used parameters to describe a typical blasting record. PPV was found to be well correlated with structural damages. Ground vibration

caused by blast loads is different from earthquakes with its characteristics of higher frequencies and shorter durations.

Ground vibration characteristics usually depend on many parameters. The parameters to be considered are [2];

(1) Weapon type and size,

(2) Properties of medium in which the structure is buried, and

(3) Depth of burst.

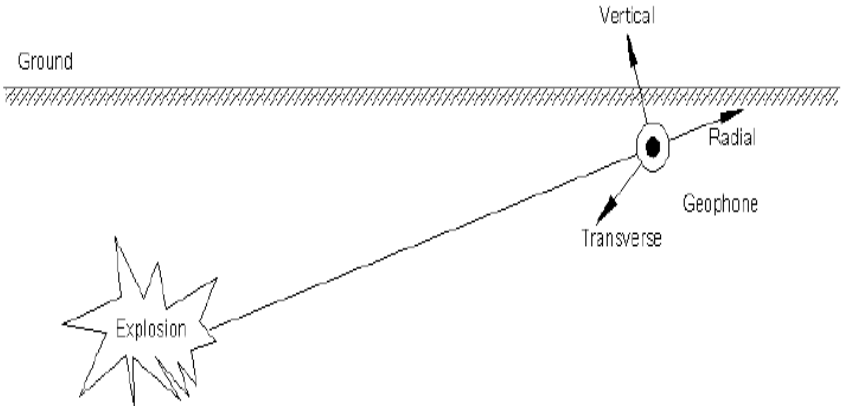


**Figure 2.5: Blast explosion and ground vibration [15].**

Project-specific attenuation relations for ground motion are geology-sensitive. Site investigation is a fundamental work for determination of ground motion characteristics under blasting practices. Blasting induced ground motions are usually recorded using geophones in terms of particle velocity. It is related to displacement and acceleration by integration and differentiation [5]. The recorded ground motion data are valuable for statistical analysis of ground vibration characteristics in terms of response spectra, which are necessary for structural spectrum analysis. For critical structures, a step-by-step time history analysis is preferred. The accelerogram data can be used as direct external excitation inputs in structural time history analysis [8].

Different methodologies have been utilized to predict blasting induced ground motions. Empirical expressions based on the collection of blast data are most commonly found in publications.

M.Y.H. Bangash (1993) in his book titled as 'Shock, Impact and Explosion, Structural Analysis and Design' gives equations to predict overpressure and the maximum mass velocity. The procedures are discussed below in detail.

The wave profile in soils is dependent upon soil type, time and distance of the source. It is widely believed that up to a distance of 100–120 $\gamma_s$ ($\gamma_s$ being equal to $R_w$, the radius of the charge), the charge weight $W$ follows the relation;

$$w = \frac{4}{3}\pi\rho_w R_w^3, \tag{2.1}$$

Where; $\rho_w$ is the density of the charge.

Here the maximum overpressure is higher than the absolute value of the under pressure due to rarefaction. At a distance of 400–500 $R_w$, the overpressure is low and is of the same order as the absolute value of the under pressure of the rarefaction wave. The zone of the fissures does not exceed 5–6 $R_w$. Just before the fissure zone, the crushing zone generally extends from 2 to 3 $R_w$. The explosive wave in an unbounded rock medium obeys the law of model similarity; the overpressure duration ( $t/R_w$)× $10^3$ on the relative distance $\overline{X} = X/R_w$ is written for a spherical PETN charge as;

$$\frac{t}{R_w} = 10^{-3}(\alpha_0 + \alpha_1 \overline{X}), \tag{2.2}$$

Where the values of constants are;

$\alpha_0$ = 2.51 for diabase with $\alpha_1$ = 4.56 × 10−3

$\alpha_0$ = 3.18 for marble with $\alpha_1$ = 5.30 × 10−2

$\alpha_0$ = 4.38 for granite with $\alpha_1$ = 0.135

$\alpha_0$ = 4.10 for water-saturated limestone with $\alpha_1$ =0.192

The corresponding overpressure can be written as;

$$p_{S0} = (\frac{a_1 \times 10^3}{\overline{X^3}} + \frac{a_2 \times 10^3}{\overline{X^2}} + \frac{a_3}{\overline{X}}) \times 10^2 . \quad (2.3)$$

The value of $a_1$, $a_2$ and $a_3$ are given below:

**Table 2.1:Values of parameters $a_1$, $a_2$ and $a_3$ [1].**

| Rock | $a_1$ | $a_2$ | $a_3$ |
|---|---|---|---|
| Diabase | 18.60 | 88.80 | 202.00 |
| Marble | 1.68 | 4.70 | 46.67 |
| Granite | 1.28 | 20.00 | 38.60 |
| Saturated limestone | -1.50 | 21.30 | -3.91 |

Under the same PETN charge, the maximum mass velocity, $\upsilon_m$, is computed as;

$$\upsilon_m = \frac{\overline{\alpha_1}}{\overline{X^3}} + \frac{\overline{\alpha_2}}{\overline{X^2}} + \frac{\overline{\alpha_3}}{\overline{X}} cms^{-1} \quad (2.4)$$

For granite, $\overline{\alpha_1}$ = 33,100 cm $s^{-1}$; $\overline{\alpha_2}$ = −398 cm $s^{-1}$; $\overline{\alpha_3}$ = 36.25 cm $s^{-1}$. For other soils where $\overline{X}$ > 50, all constants become equal for all kinds of explosives.

Theodor Krauthammer (2008) also in his books gives equations to predict peak displacement, time dependent particle velocity, time dependent pressure and peak ground acceleration. The general theoretical procedures are explained in detail here below.

Beyond the peak, the pulse decays to the ambient pressure or velocity (assumed to be zero) are estimated according the following expressions:

$$P(t) = P_0 e^{\frac{\alpha t}{t_a}} \quad t \geq 0 \quad (2.5)$$

$$V(t) = V_0 (1 - \frac{\beta t}{t_a}) e^{\frac{-\beta t}{t_a}} \quad t \geq 0 \quad (2.6)$$

Where;

- P(t) is the pressure,
- V(t) is the particle velocity,

- $P_0$ is the corresponding peak pressure,
- Vo is the corresponding peak velocity, and
- α and β are the following time constants:

$$\alpha = 1.0, \beta = \frac{1}{2.5} \tag{2.7}$$

The time of arrival $t_a$ is the time for a ground shock to reach a given location and is computed as follows:

$$t_a = \frac{R}{c} \tag{2.8}$$

$$c = \left(\frac{M}{\rho_0}\right)^{\frac{1}{2}} \tag{2.9}$$

Where;

- R is the range or scaled standoff distance,
- c is the average seismic velocity over that range,
- M is the stiffness (modulus) of the soil,
- $\rho_0$ is its mass density.

The following relationships can be employed for bombs detonating on or in burster slabs, or in the soil near a target;

$$P_0 = f.(\rho c).160\lambda^{-n} \tag{2.10}$$

$$V_0 = f.160.\lambda^{-n} \tag{2.11}$$

$$W^{\frac{1}{3}}.A_0 = f.50.c.\lambda^{(-n-1)} \tag{2.12}$$

$$W^{\frac{1}{3}}.D_0 = f.\frac{500}{c}.\lambda^{(-n-1)} \tag{2.13}$$

$$\lambda = \frac{R}{W^{\frac{1}{3}}}, \tag{2.14}$$

Where;

- f is the coupling factor,
- $\rho c$ is the acoustic impedance (pounds per square inch/feet per second),
- R is the range (feet),
- W is the charge weight (pounds),
- n is the attenuation coefficient,
- Vo is the peak particle velocity (feet per second),
- $a_o$ is the peak (gravitational or g) acceleration,
- c is the seismic velocity (feet per second),
- $d_o$ equals peak displacements.

Some typical values of soil properties for various materials are presented in Table 2.2 and Fig 2.6. Users should obtain actual values for a site under consideration.

In all cases, an appropriate coupling factor f must be chosen. This factor represents the degree of energy transfer into the medium, as compared to the case of a fully contained explosion. For explosions in air, it is assumed that f = 0.14 and is assumed to be constant for detonations near the ground surface. Fig 2.4 should be used to select the coupling factor for explosives in soil and concrete.

**Table 2.2:Soil Properties for Calculating Ground Shock Parameters [2].**

| Material Description | Seismic Velocity c (fps) | Impedance c (psi/fps) | Attenuation Coefficient (n) |
|---|---|---|---|
| Loose, dry sands and gravels with low relative Density | 600 | 12 | 3−3.25 |
| Sandy loam, loess, dry sands, and backfill | 1000 | 22 | 2.75 |
| Dense sand with high relative density | 1600 | 44 | 2.5 |
| Wet sandy clay with air voids (less than 1%) | 1800 | 48 | 2.5 |
| Saturated sandy clays and sands with small number of air voids (less than 1%) | 5000 | 130 | 2.25-2.5 |
| Heavy saturated clays and clay shales | >5,000 | 150-180 | 1.5 |

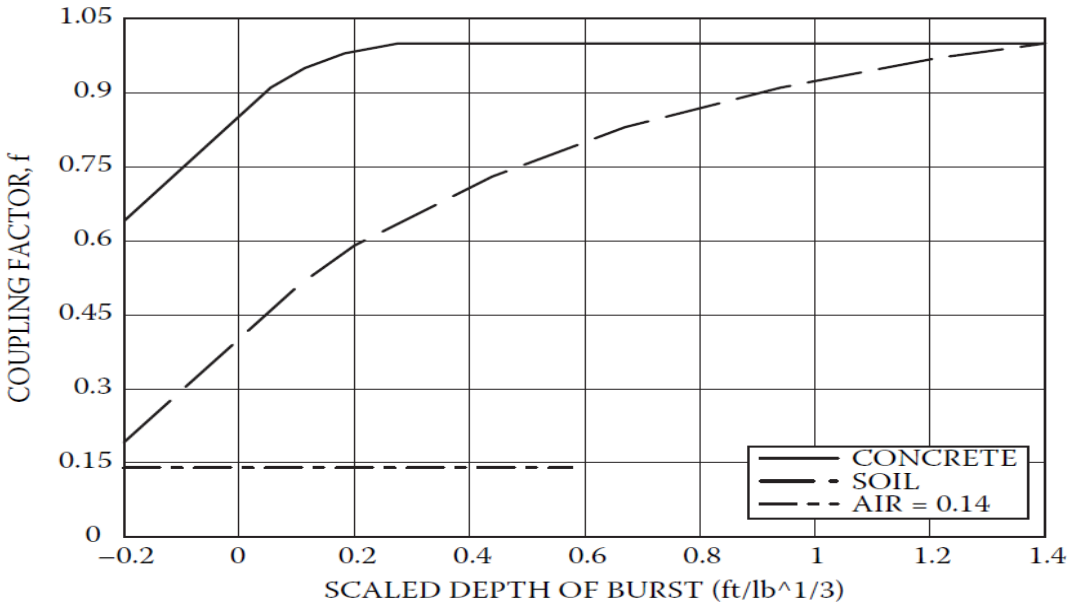


**Figure 2.6:Ground shock coupling factor as function of scaled depth of burst [2].**

Dowing (1985) in his book gives equations to predict peak particle velocity based on cube root scaling relationships derived from field measurements.

He assumes that charge weight per delay is W; distance from blast to structure is R; rock density is $\rho$ ; then peak particle velocity, $\dot{u}$ is given by:

$$\dot{u} = 0.72\left(\frac{100}{R}\right)^{1.46}\left(\frac{W}{10}\right)^{0.48}\left(\frac{4.66}{\rho}\right)^{0.48} \tag{2.15}$$

It is explained above that empirical formulas given by M.Y.H. Bangash and Dowing enables us to calculate peak values of blast induced ground motions. But the empirical formulas given by Theodor Krauthammer enables us to predict both peak and time dependent blast induced ground motions. It is also shown that the applicability of M.Y.H. Bangash's empirical formula is limited to some ground types as given in table 2.1. But Theodor Krauthammer and Dowing's empirical formulas are applicable to all ground types. The above discussion generalizes that Theodor Krauthammer's empirical formula is more general because it's applicable to all soil types and it enables us to calculate both peak and time dependent blast induced ground motions. Because of this generality it is used in this thesis work for ground motion generations.

In this thesis work blast induced ground motion in terms of velocity time history is generated using equation 2.6 assuming the explosion occurred in sandy soil with high density and the target structure located at 4m,7m and 10m. The generated velocity time history is shown below in Figs 2.7, 2.8 and 2.9 for 4m, 7m and 10m stand of distance respectively.

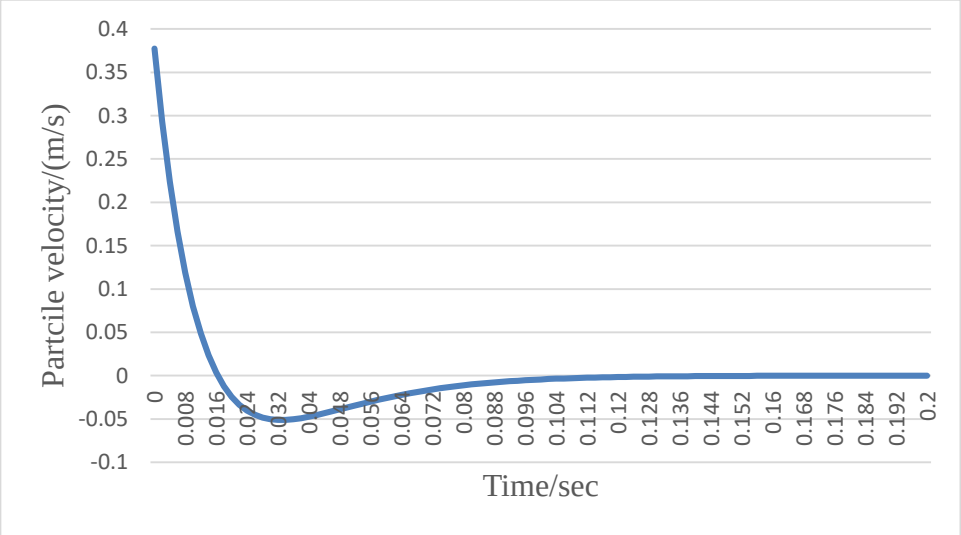


**Figure 2.7: Velocity time history at 4m standoff distance.**

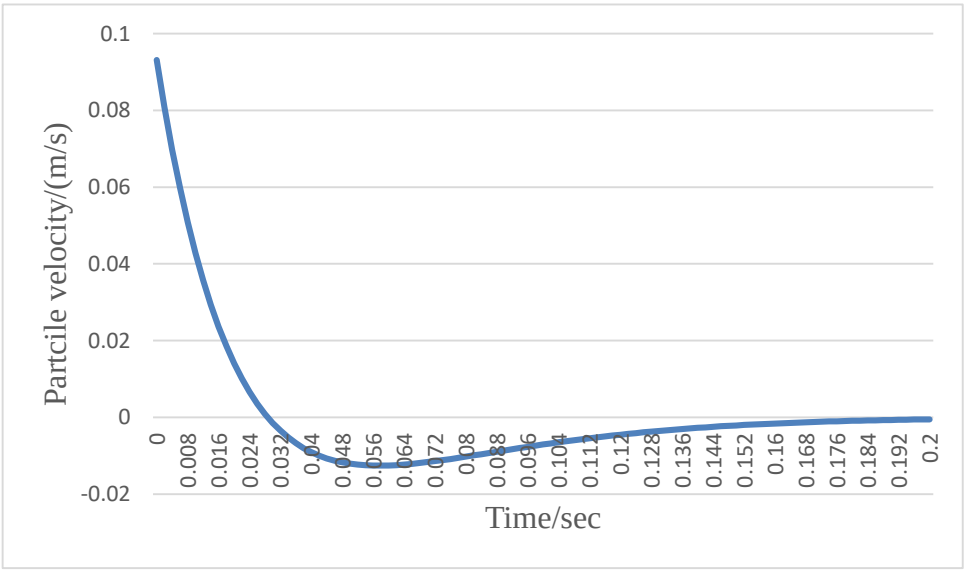


**Figure 2.8 : Velocity time history at 7m standoff distance.**

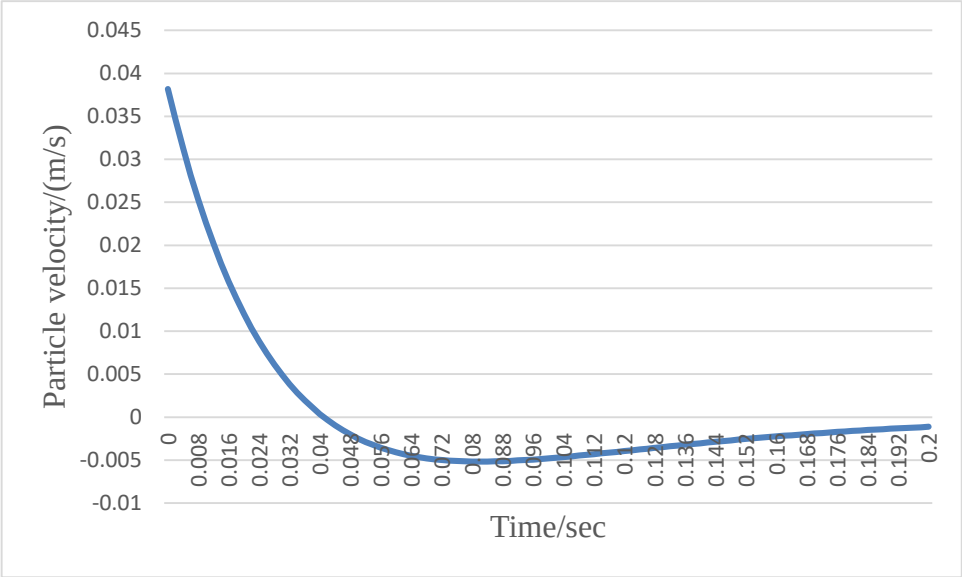


**Figure 2.9: Velocity time history at 10m standoff distance.**

### 2.5.1 Signal integration and differentiation

Numerical integration and differentiation were performed to generate target data that could not be obtained from direct measurement. In this thesis work the raw data which can be generated by using procedure outlined above is time domain velocity signal. Therefore, it can be either integrated into displacement time history or differentiated into acceleration time domain data. Numerical integration scheme in time domain is straightforward: assuming x(n), (n=0,1,2….N) is the measured signal, and Δt is integration time step, then y(n) which is the integral of X(n) can be calculated using the Trapezoidal rule ( Manassah 2001): [7]

$$\{y(n)\} = \Delta t \sum_{k=1}^{n} \frac{x(k-1)+x(k)}{2} \quad (n=1,2,\ldots.N) \tag{2.16}$$

Numerical differentiation is to estimate the derivative of a signal using recorded discrete values. A simple two-point estimation was used to compute y(n) which is the differentiation of input signal x(n), (n=0,1,2…. N) With time step, Δt (Manassah 2001): [7]

$$y(n) = \frac{[x(n)-x(n-1)]}{\Delta t} \tag{2.17}$$

## 2.6 Material behavior at high strain rate

The behaviour of materials used under blast application depends on their mechanical properties under such high strain rates of loadings. It has been well documented that material stress-strain behaviour is greatly influenced by strain rates. Under high strain rates, the materials exhibit stiffer constitutive behaviour, resulting in improved mechanical properties [3]. Fig. 2.10 shows strain-associated loading.

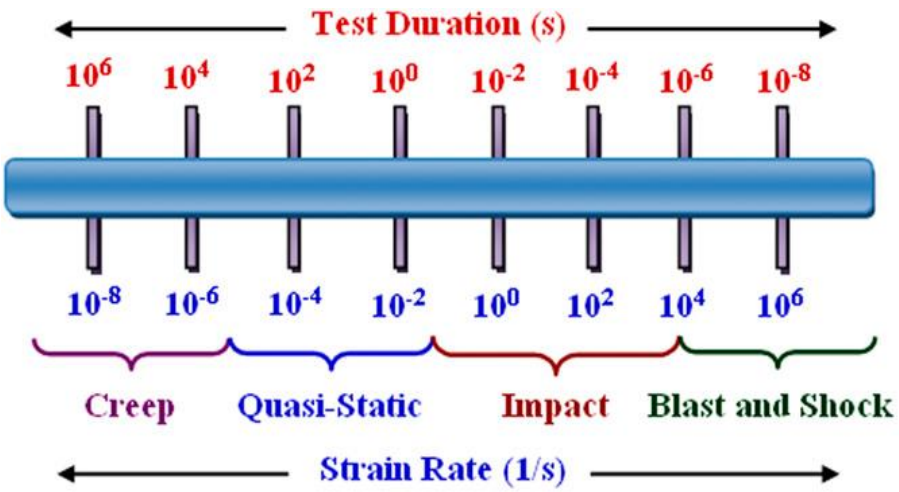


**Figure 2.10: Strain rates associated with different types of loading [20].**

A structural element subjected to a blast loading exhibits a higher strength than a similar element subjected to a static loading. This increase in strength for both the concrete and reinforcement is attributed to the rapid rates of strain that occur in dynamically loaded members. These increased stresses or dynamic strengths are used to calculate the element's dynamic resistance to the applied blast load. Thus, the dynamic ultimate resistance of an element subjected to a blast load is greater than its static ultimate resistance. Both the concrete and reinforcing steel exhibit greater strength under rapid strain rates. The higher the strain rate, the higher the compressive strength of concrete and the higher the yield and ultimate strength of the reinforcement. This phenomenon is accounted for in the design of a blast resistant structure by using dynamic stresses to calculate the dynamic ultimate resistance of the reinforced concrete members [12,2]. The dynamic increase factors for design and analysis of (RC) reinforced concrete structures are presented below.

**Table 2.3: Reinforced Concrete Design Dynamic Increase Factors [10].**

| Type of Stress | Far-In Design Range | | | Close-In Design Range | | |
|---|---|---|---|---|---|---|
| | Reinforcing Bars | | Concrete | Reinforcing Bars | | Concrete |
| | $f_{dy}/f_y$ | $f_{du}/f_u$ | $f'_{dc}/f'_c$ | $f_{dy}/f_y$ | $f_{du}/f_u$ | $f'_{dc}/f'_c$ |
| Bending | 1.17 | 1.05 | 1.19 | 1.23 | 1.05 | 1.25 |
| Diagonal tension | 1 | — | 1 | 1.1 | 1 | 1 |
| Direct shear | 1.1 | 1 | 1.1 | 1.1 | 1 | 1.1 |
| Bond | 1.17 | 1.05 | 1 | 1.23 | 1.05 | 1 |
| Compression | 1.1 | — | 1.12 | 1.13 | — | 1.16 |

Where;

- $f_{dy}$ is Design yield strength of steel,
- $f_y$ is Yield strength of steel,
- $f_{du}$ is design ultimate strength of steel,
- $f_u$ is ultimate strength of steel,
- $f'_{dc}$ is Design uniaxial compressive strength of concrete,
- $f'_c$ is Uniaxial compressive strength of concrete ( cylinder test).

## 2.7 Previous work

Abdulaziz kasahun (2005) on his study ‘Blast loading and blast effects on RC frame buildings gives an overview to the nature of blast loading and its effects on reinforced concrete frame structures, designed to withstand normal gravity and earthquake loads. according to his study building designed according to the (EBCS) guidelines did not satisfied (UFC 2005) requirements to mitigate progressive collapse, and building designed according to the (UFC 2005) requirements could withstand blast loads result from detonation of 250 lbs (113.5 kg) at 10m standoff distance and also he found out that the maximum displacement difference ratio increases as the standoff distance decreases.

Dan (Danesh) Nourzadeha, Jagmohan Humarb and Abass Braimahb (2017) on their study titled as ‘Comparison of Response of Building Structures to Blast Loading and Seismic Excitations’ gives an explanation on response of structure for blast loads and

earth quake loads. They analysed a10-story building to moderate blast loading and several different synthetic ground motions whose spectra are comparable to different hazard spectra and they found out that consideration of global responses of a building for blast loads is important and parameters such as lateral drifts and floor responses should be considered in design and response assessment procedure for blast loading.

Mohammed S. Al-Ansari (2012) on his study 'Building response to blast and earthquake loading' points out that structural engineers need to consider blast loading in their design more frequently. He drives a relationship between blast loads and earth quake loads. He compares between the response of buildings to blast and earthquake loadings for the purpose of deriving a relationship in a form of formulae and charts between blast and earthquake loads. He obtained the numerical data using several structural models with different dimensions, shapes, and material and subjected to different blast loadings, and earthquake loads in different zones. He concludes that the derived relationship between blast and earthquake loads can be used to compute equivalent earthquake ground acceleration to a blast load on any building given the intensity of the blast, the stand-off distance, and the building height and once the earthquake ground acceleration is known, the codes of design methodology could be easily used to determine the lateral forces and design the building members accordingly.

J.R.Thonen and S.L.Windes (1942) investigated the displacements of ground and structure due to seismic waves from detonations of different amounts of explosives measured in pounds. The study is based upon data collected from records of several hundred tests conducted at 28 stone quarries situated in 11 Southern and Eastern States, in a limestone mine, and in 20 residential structures of various types. The tests covered the detonation of explosive charges in regular quarry practice ranging in weight from 1.5 to 42,000 pounds. Distances between shot point and seismometer stations ranged from 100 feet to 2 miles. Transmitting mediums through which the seismic waves were propagated ranged from granites through limestone's, shale's, and clays to unconsolidated sand and gravel beds. They found that magnitude of seismic displacement caused by quarry blasts can be predicted accurately enough for practical purposes if the weight of the explosive charge and the distance between shot point and structure are known. According to their investigations ground and structural

displacements ranged from 0.0001 to 0.06 inch for quarry shots ranging in weight of explosive charge from 4 pounds at a distance of 185 feet to 15,400 pounds at 600 feet.

Vitaly I.,et al. (1998) determined the upper limit M(Y)max for the seismic magnitude of an explosion (chemical or nuclear) at given yield Y for numerous different explosions under different conditions in hard rock and then to compare the magnitude of an explosion of interest (of known charge size or yield) with the upper magnitude limit for that yield. According to their investigations the equations found for M(Y) max is;

$M(Y)m = 2.45 + 0.73\log Y$ , where Y is the yield in (tons) (2.18)

$= 4.64 + 0.73\log Y$ , where Y is the yield in (kilo tones) (2.19)

Then after analyzing the equations for different charge sizes and interpreting the results; they found that typical chemical explosions carried out by the mining and construction industries are efficient at generating seismic signals as compared to the upper limit.

# CHAPTER 3 ANALYSIS METHODS FOR BLAST LOADING

## 3.1 Introduction

Structural elements must develop an internal resistance sufficient to maintain all motion within the limits of deflection prescribed for the particular design. The load capacity of the member depends on the peak strength developed by the specific member and on the ability of the member to sustain its resistance for a specific though relatively short period of time [10]. This section describes the methods used for the analysis of structural elements subjected to dynamic loads. Common methods/approaches for blast analysis are discussed below.

## 3.2 Equivalent static methods

One method of blast analysis which had been commonly used in the past, but which is no longer advocated is the equivalent static method [13]. The method employs a static analysis with an approximate applied load to simulate the dynamic response. Dynamic parameters such as time varying loads, rapid strain rate material strengths, load amplification factors, mass, stiffness, period of vibration, and allowable plastic deformations are not used. The primarily difficulty with this method is determining an appropriate static loading which will yield reasonable results. This method is not recommended for general use except for cases where the structure is far removed from the blast source, such that the blast loading resembles a wind gust.

## 3.3 Single-Degree-of-Freedom Systems

A single degree of freedom system is one in which only one coordinate is essential to define its motion [10]. If a system is constrained such that it can vibrate in only one mode with a single co-ordinate system (geometric location of the masses within the system), then it is a single-degree-of-freedom system [1].

Complexity in analyzing the dynamic response of blast-loaded structures involves the effect of high strain rates, the non-linear inelastic material behavior, the uncertainties of

blast load calculations and the time-dependent deformations. Therefore, to simplify the-analysis, a number of assumptions related to the response of structures and the loads has been proposed and widely accepted. To establish the principles of this analysis, the structure is idealized as a single degree of freedom (SDOF) system and the link between the positive duration of the blast load and the natural period of vibration of the structure is established. This leads to blast load idealization and simplifies the classification of the blast loading regimes [27].

### 3.3.1 Elastic SDOF Systems

The simplest discretization of transient problems is by means of the SDOF approach. The actual structure can be replaced by an equivalent system of one concentrated mass and one weightless spring representing the resistance of the structure against deformation. Such an idealized system is illustrated in Fig 3.1. The structural mass, M, is under the effect of an external force, F(t), and the structural resistance, R, is expressed in terms of the vertical displacement, y, and the spring constant, K. The blast load can also be idealized as a triangular pulse having a peak force $F_m$ and positive phase duration $t_d$ (see Fig 3.1). The forcing function is given as;

$$F(t) = F_m\left(1-\frac{t}{t_d}\right) \tag{3.1}$$

The blast impulse is approximated as the area under the force-time curve, and is given by;

$$I = \frac{1}{2}F_m t_d \tag{3.2}$$

The equation of motion of the un-damped elastic SDOF system for a time ranging from 0 to the positive phase duration, $t_d$, is given by Biggs (1964) as;

$$M\ddot{y} + Ky = F_m\left(1-\frac{t}{t_d}\right) \tag{3.3}$$

The general solution can be expressed as:

$$\text{Displacement, } y(t) = \frac{F_m}{K}(1-\cos\omega t) + \frac{F_m}{Kt_d}\left(\frac{\sin\omega t}{\omega} - t\right) \tag{3.4}$$

$$\text{Velocity, } \dot{y}(t) = \frac{dy}{dt} = \frac{F_m}{K}\left[\omega\sin\omega t + \frac{1}{t_d}(\cos\omega t - 1)\right] \tag{3.5}$$

Where;

- $\omega$ is the natural circular frequency of vibration of the structure which is given by;

$$\omega = \frac{2\Pi}{T} = \sqrt{\frac{K}{M}} \tag{3.6}$$

$T$ is the natural period of vibration of the structure.

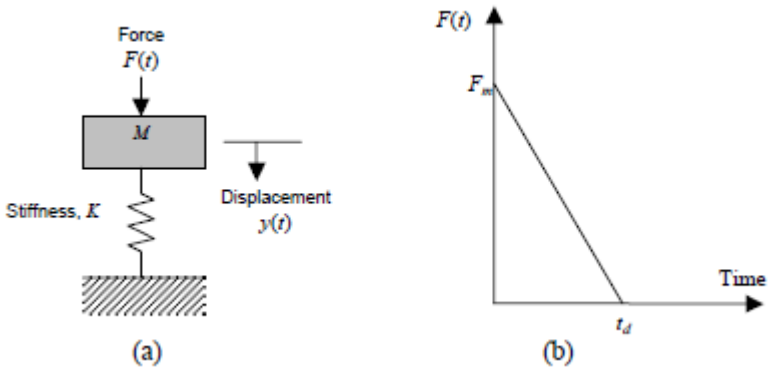


**Figure 3.1: (a) SDOF system and (b) blast loading [27].**

The maximum response is defined by the maximum dynamic deflection $y_m$ which occurs at time $t_m$. The maximum dynamic deflection $y_m$ can be evaluated by setting $dy/dt$ in Equation 3.4 equal to zero, i.e. when the structural velocity is zero. The dynamic load factor, DLF, is defined as the ratio of the maximum dynamic deflection $y_m$ to the static deflection $y_{st}$ which would have resulted from the static application of the peak load $F_m$, which is shown as follows:

$$DLF = \frac{y_{\max}}{y_{st}} = \frac{y_{\max}}{F_m/K} = \psi(\omega t_d) = \Psi\left(\frac{t_d}{T}\right) \tag{3.7}$$

The structural response to blast loading is significantly influenced by the ratio $t_d/T$ or $\omega$ td ($t_d/T = \omega t_d/2\pi$ ).

Three loading regimes are categorized as follows:

- $\omega t_d < 0.4$ : impulsive loading regime.

- $\omega t_d > 40$ :quasi-static loading regime.

- $0.4 < \omega t_d < 40$ : Dynamic loading regime.

### 3.3.2 Elasto-Plastic SDOF Systems

Structural elements are expected to undergo large inelastic deformation under blast load or high velocity impact. Nonlinear dynamic analysis techniques are similar to those currently used in advanced seismic analysis. Analytical models range from equivalent single-degree-of-freedom (SDOF) models to finite element (FE) representation. For SDOF and FE methods, numerical computation requires adequate resolution in space and time to account for the high-intensity, short-duration loading and nonlinear response (Fig 3.2). Difficulties involve the selection of the model, and appropriate failure modes, and finally, the interpretation of the results for structural design details. Exact analysis of dynamic response is then only possible by step-by-step numerical solution requiring nonlinear dynamic finite- element software. Components such as beams, slabs, or walls can often be modeled by a SDOF system and the governing equation of motion solved by using numerical methods. There are also charts available in text books and military handbooks for linearly decaying loads, which provide the peak response and simplify the need to solve differential equations [16].

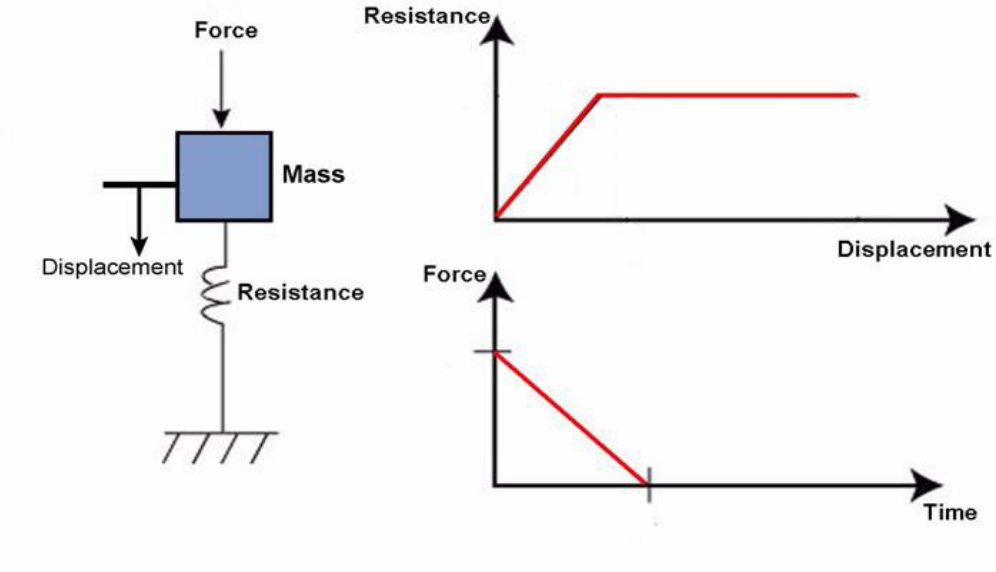


**Figure 3.2: Simplified elasto-plastic SDOF model for blast load [16].**

For an inelastic system the equation of motion to be solved numerically is;

$$m\ddot{u} + c\dot{u} + f_s(u) = p(t) \quad \text{or} \quad -m\ddot{u}_g(t) \tag{3.8}$$

Subject to the initial conditions;

$$u_0 = u(0) \qquad \dot{u}_0 = \dot{u}(0) \tag{3.9}$$

The applied force p (t) is given by a set of discrete values $p_i = p(t_i)$, i = 0 to N

The time interval is given by the formula;

$$\Delta t_i = t_{i+1} - t_i \tag{3.10}$$

The response is determined at the discrete time instants $t_i$ , denoted as time i ; the displacement, velocity, and acceleration of the SDF system are $u_i$, $\dot{u}_i$ , and $\ddot{u}_i$, respectively. These values, assumed to be known, satisfy Eq. (3.8) at time i given as:

$$m\ddot{u}_i + c\dot{u}_i + (f_s)_i = p_i \tag{3.11}$$

Where $(f_s)_i$ is the resisting force at time i. The numerical procedures to be presented will enable us to determine the response quantities $u_{i+1}$, $\dot{u}_{i+1}$, and $\ddot{u}_{i+1}$ at time i + 1 that satisfy Eq. (3.8) at time i + 1 given as:

$$m\ddot{u}_{i+1} + c\dot{u}_{i+1} + (f_s)_{i+1} = p_{i+1} \tag{3.12}$$

When applied successively with i = 0, 1, 2, 3. . . , the time-stepping procedure gives the desired response at every time instants i = 1, 2, 3, . . . . The known initial conditions, $u_0 = u(0)$ and $\dot{u}_0 = \dot{u}(0)$ provide the information necessary to start the procedure.

The response of the ideal elasto-plastic system can be evaluated using:

(a) Graphical presentations of solutions

As noted above, analytical solutions for SDOF systems may be very cumbersome, even for simple loading functions. Such computations become much harder for nonlinear resistance functions and complicated loading pulses. To simplify such computations in support of design activities, one may use dynamic response charts that enable an analyst to estimate the values of key parameters for assessing the suitability of a tentative structural design. As illustrated in Fig 3.2 for a right angle triangular load and an assumed elasto-plastic resistance function, Fig 3.3 illustrates a family of curves that relate the ductility factor μ to the non-dimensional time ratio $t_d/T$ (pulse duration to natural period).

Each curve represents a different yield resistance to peak load ratio $R_m/F_1$. For a tentative design, one knows the values of $t_d/T$, $R_m/F_1$, and the peak elastic deflection $y_{el}$. These values will define uniquely the ductility factor μ from which one computes the maximum displacement $y_m$. The derived value of $y_m$ can be used to assess the adequacy of the selected design. For example, if $y_m$ is the peak displacement for a beam, dividing it by half the span length L/2 yields the support rotation θ. Comparing the derived support rotation with recommended damage levels will show whether the beam will meet its performance or operational requirements.

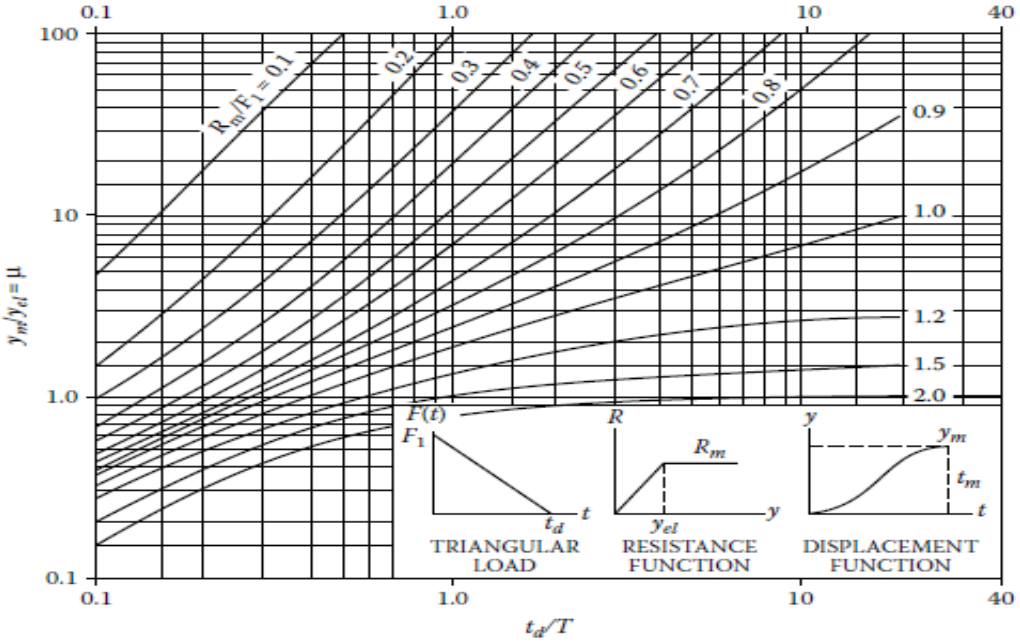


**Figure 3.3: Maximum response of elasto-plastic SDOF systems under triangular load pulse with zero rise time [10].**

(b) Closed Form Solutions

They are available only for some simple loading cases of SDOF systems. Published solutions exist for both elastic and elastic-plastic responses, and for triangular and rectangular load pulses. The analysis can also be greatly simplified when the duration of the loading, $t_d$, is either very short or extremely long compare to the period, $t_n$ [13].

(c) Numerical solutions

The closed form solution of the equation of motion by the approach described earlier may not be possible for highly nonlinear cases. Furthermore, it is necessary to derive an efficient numerical integration procedure that will be valid for a wide range of cases. One such technique is the Newmark numerical integration method, which is commonly used to obtain the time history response for nonlinear SDOF systems.

Recall that this method determines the solution at time i + 1 from the equilibrium condition at time i + 1, i.e., Eq. (3.12) for nonlinear systems. Because the resisting force $(f_s)_{i+1}$ is an implicit nonlinear function of the unknown $u_{i+1}$, iteration is required in this method. This requirement is typical of implicit methods. It is instructive first to develop the Newton–Raphson method of iteration for static analysis of a nonlinear SDF system [5].

**Newton–Raphson Iteration**

Dropping the inertia and damping terms in the equation of motion Eq. (3.8) gives the nonlinear equation to be solved in a static problem:

$$f_s(u) = p \tag{3.13}$$

The task is to determine the deformation u due to a given external force p, where the nonlinear force–deformation relation $f_s(u)$ is defined for the system to be analysed.

Suppose that after j cycles of iteration, $u^j$ is an estimate of the unknown displacement and we are interested in developing an iterative procedure that provides an improved estimate $u^{j+1}$.

For this purpose after expanding $(f_s)_{i+1}$ in Taylor series about the known estimate $u^j$ *and neglecting* the higher order terms;

$$f_s^{(j+1)} \approx f_s^{(j)} + k_T^{(j)} \Delta u^{(j)} = p \tag{3.14}$$

$$k_T^{(j)} u^j = p - f_s^{(j)} = R^{(j)} \tag{3.15}$$

Where;

- $k_T^{(J)}$ is the tangent stiffness at $u^j$
- $R^j$ is the residual force.

The iterative procedure is outlined below.

1. Associated with $u^j$ is the force $f_s^{(j)}$, which is not equal to the applied force p, and a residual force is defined as:

$$R^j = p - f_s^{(j)}$$

2. The additional displacement due to this residual force is;

$$\Delta u^j = \frac{R^j}{k_T{}^J}$$

3. Now displacement at j+1, is;

$$u^{j+1} = u^j + \Delta u^j$$

4. Calculate the new value of $R^{j+1}$

$$R^{j+1} = p - f_s^{(j+1)}$$

5. Calculate additional displacement at j+1

$$\Delta u^{(j+1)} = R^j + \frac{1}{k_T{}^{(j+1)}}$$

6. Now displacement at j+2 is

$u^{(j+2)} = u^{(j+1)} + \Delta u^{(j+1)}$ …., the process continued until convergence is achieved.

**Newmark's Method**

In 1959, N. M. Newmark developed a family of time-stepping methods based on equations 3.12 and the following equations [5]:

$$\dot{u}_{i+1} = \dot{u}_i + \left[(1-\gamma)\Delta t\right]\ddot{u}_i + (\gamma\Delta t)\ddot{u}_{i+1} \tag{3.16}$$

$$u_{i+1} = u_i + (\Delta t)\dot{u}_i + \left[(0.5-\beta)(\Delta t)^2\right]\ddot{u}_i + \left[\beta(\Delta t)^2\right]\ddot{u}_{i+1} \tag{3.17}$$

The parameters β and γ define the variation of acceleration over a time step and determine the stability and accuracy characteristics of the method. Typical selection for γ is 1/2, and 1/6≤ β ≤ ¼ is satisfactory from all points of view, including that of accuracy. These two equations, combined with the equilibrium equation (3.12) at the end of the time step, provide the basis for computing $u_{i+1}$, $\dot{u}_{i+1}$, and $\ddot{u}_{i+1}$ at time i + 1 from the known $u_i, \dot{u}_i$, and $\ddot{u}_i$ at time i . Iteration is required to implement these computations because the unknown $\ddot{u}_{i+1}$ appears in the right side of Eq. (3.12). We have developed Newton–Raphson iteration to solve a nonlinear equilibrium equation [e.g., Eq. (3.13)] that governs the static problem.

In dynamic analysis the goal is to determine response quantities $u_{i+1}$, $\dot{u}_{i+1}$, and $\ddot{u}_{i+1}$ at time i + 1 that satisfy Eq. (3.12), which can be written as;

$$\left(\hat{f}_s\right)_{i+1} = p_{i+1} \tag{3.18}$$

Where;

$$\left(\hat{f}_s\right)_{i+1} = m\ddot{u}_{i+1} + c\dot{u}_{i+1} + \left(f_s\right)_{i+1} \tag{3.19}$$

By including the inertia and damping forces in defining the "resisting force" $\hat{f}_s$, the dynamic analysis equation (3.18) is of the same form as the static analysis equation (3.13). Thus, by adapting the Taylor series expansion of Eq. (3.18), and dropping the second- and higher-order terms, we can obtain an equation analogous to Eq. (3.14):

$$(\hat{f}_s)_{i+1}^{j+1} \approx (\hat{f}_s)_{i+1}^{(j)} + \frac{\partial \hat{f}_s}{\partial u_{i+1}} \Delta u^{(j)} = p_{i+1} \tag{3.20}$$

Where;

$$\Delta u^{(j)} = u_{i+1}^{(j+1)} - u_{i+1}^{(j)} \tag{3.21}$$

Differentiating Eq. (3.19) at the known displacement $u_{i+1}^{j}$ gives;

$$\frac{\partial \hat{f}_s}{\partial u_{i+1}} = m\frac{\partial \ddot{u}}{\partial u_{i+1}} + c\frac{\partial \dot{u}}{\partial u_{i+1}} + \frac{\partial f_s}{\partial u_{i+1}} \tag{3.22}$$

Where the derivatives in inertia and damping terms on the right side can be determined from Newmark's equations, Eq. (3.16 and 3.17);

$$\frac{\partial \ddot{u}}{\partial u_{i+1}} = \frac{1}{\beta(\Delta t)^2} \qquad \frac{\partial \dot{u}}{\partial u_{i+1}} = \frac{\gamma}{\beta \Delta t} \tag{3.23}$$

Putting together the preceding two equations and recalling the definition of tangent stiffness gives;

$$(\hat{k}_T)_{i+1}^{(j)} \equiv \frac{\partial \hat{f}_s}{\partial u_{i+1}} = (\hat{k}_T)_{i+1}^{(j)} + \frac{\gamma}{\beta \Delta t}c + \frac{1}{\beta(\Delta t)^2}m \tag{3.24}$$

With the preceding definition of $(k_T)_{i+1}^{j}$, Eq. (3.20) can be written as;

$$(\hat{k}_T)_{i+1}^{(j)} \Delta u^{(j)} = p_{i+1} - (\hat{f}_s)_{i+1}^{j} \equiv \hat{R}_{i+1}^{(j)} \tag{3.25}$$

Substituting newmarks Eq. (3.16 and 3.17) and then combining it with the right side of Eq. (3.25) leads to the following expression for the residual force;

$$\hat{R}_{i+1}^{(j)} = p_{i+1} - (f_s)_{i+1}^{(j)}\left[\frac{1}{\beta(\Delta t)^2}m + \frac{\gamma}{\beta \Delta t}c\right](u_{i+1}^{(j)} - u_i) + \left[\frac{1}{\beta \Delta t}m + \left(\frac{\gamma}{\beta} - 1\right)c\right]\dot{u}_i + \left[\left(\frac{1}{2\beta} - 1\right)m + \Delta t\left(\frac{\gamma}{2\beta} - 1\right)c\right]\ddot{u}_i \tag{3.26}$$

Newmark's algorithm for both linear and non-linear systems are summarized below.

The algorithm for the step by step Newmark's linear acceleration method of a single degree of freedom system is outlined below [13]:

1. Determine the stiffness, K, mass, M, damping coefficient, C, force function F(t), Maximum restoring force , Rt, and time increment, Δt.

2. At each time step (step =0 to end), determine the value of the forcing function, $F_o \ldots F_{end}$.
3. For the initial time step (step=0), initialize the displacement, velocity and acceleration.

   $y_o=0$; $v_o=0$; $a_o=F_o/M$

4. For each time (step =i ,beginning with i=0)

- Calculate the effective stiffness,

$$K_i = K + (\frac{6}{\Delta t^2})M + (\frac{3}{\Delta t})C$$

- Calculate the effective incremental force,

$$\Delta F_i = (F_{i+1} - F_i) + \left[ (\frac{6}{\Delta t})M + (3)C \right] y_i + \left[ (3)M + (\frac{\Delta t}{2})C \right] a_i$$

- Solve for the incremental displacement,

$$\Delta y_i = \frac{\Delta F_i}{K_i},$$

- Calculate the incremental velocity,

$$\Delta y_i = (\frac{3}{\Delta t})\Delta y_i - (3)a_i - (\frac{\Delta t}{2})a_i$$

- Calculate the displacement , and velocity at the next time step (step=i+1)

  $y_{i+1}=y_i+ \Delta y_i$

  $v_{i+1}=vi+ \Delta v_i$

- Calculate the acceleration $a_{i+1}$ at the end of the time interval using the dynamic equation of equilibrium:

$$a_{i+1} = (\frac{1}{M})\left[F_{i+1} - (C_{i+1})(v_{i+1}) - \left[R_t - (y_i - y_{i+1})\right]K\right]$$

5. Repetition for the next time steps

Newmark's algorithm for non- linear system [5].

Special cases;

(1) Average acceleration method ( $\gamma = \frac{1}{2}, \beta = \frac{1}{4}$ )

(2) Linear acceleration method ( $\gamma = \frac{1}{2}, \beta = \frac{1}{6}$ )

1.0 Initial calculations

1.1 State determinations: $(f_s)_0$ and $(k_T)_0$.

1.2 $\ddot{u}_0 = \frac{p_0 - c\dot{u}_0 - (f_s)_0}{m}$

1.3 Select $\Delta t$

1.4 $a_1 = \frac{1}{\beta(\Delta t)^2} m + \frac{\gamma}{\beta \Delta t} c; a_2 = \frac{1}{\beta \Delta t} m + \left( \frac{\gamma}{\beta} - 1 \right)$ and

$$a_3 = (\frac{1}{2\beta} - 1)m + \Delta t(\frac{\gamma}{2\beta} - 1)c.$$

2.0 Calculations for each time instant, i = 0, 1, 2, . . .

2.1 Initialize $j = 1, u_{i+1}^{(j+1)} = u_i, (f_s)_{i+1}^{(j)} = (f_s)_i$ and $(k_T)_{i+1}^{j} = (k_T)_i$

2.2 $\hat{p}_{i+1} = p_{i+1} + a_1 u_i + a_2 \dot{u}_i + a_3 \ddot{u}_i.$

3.0 For each iteration, j = 1, 2, 3 . . .

3.1 $R_{i+1}^{(j)} = \hat{p}_{i+1} - (f_s)_{i+1}^{(j)} - a_1 u_{i+1}^{(j)}$

3.2 check convergence;if the acceptance criteria are met, implement steps

3.3 to 3.7; otherwise, skip these steps and go to step 4.0.

3.3 $(\hat{k}_T)_{i+1}^{(j)} = (k_T)_{i+1}^{(j)} + a_1$

3.4 $\Delta u^j = \hat{R}_{i+1}^{(j)} \div (\hat{k}_T)_{i+1}^{(j)}.$

3.5 $(u)_{i+1}^{(j+1)} = (u)_{i+1}^{(j)} + \Delta u^{(j)}$

3.6 state determinations: $(f_s)_{i+1}^{(j+1)}$ and $(k_T)_{i+1}^{(j+1)}$.

3.7 Replace j by j+1 and repeat steps 3.1 to 3.6; denote final value as $u_{i+1}$.

4.0 Calculations for velocity and acceleration

4.1 $\dot{u}_{i+1} = \frac{\gamma}{\beta\Delta t}(u_{i+1} - u_i) + (1 - \frac{\gamma}{\beta})\dot{u}_i + \Delta t(1 - \frac{\gamma}{2\beta})\ddot{u}_i$

4.2 $\ddot{u}_{i+1} = \frac{1}{\beta(\Delta t)^2}(u_{i+1} - u_i) - \frac{1}{\beta\Delta t}\dot{u}_i - (\frac{1}{2\beta} - 1)\ddot{u}_i.$

5.0 Repetition for next time step. Replace i by i + 1 and implement steps 2.0 to

4.0 for the next time step.

## 3.4 Finite element analysis method

The finite element method is one of the most important developments in applied mechanics [5]. A finite element analysis method is recommended when one or more of the following conditions exist [13].

a) The ratio of a member's natural frequency to the natural frequency of the support system is in range of 0.5 to 2.0, such that an uncoupled analysis approach may yield significant inaccurate result.

b) Overall structural behaviour is to be evaluated with regard to structural stability, gross displacements and P-delta effects.

c) The structure has unusual features such as unsymmetrical or no uniform mass and stiffness characteristics.

Many commercial finite element programs are available for nonlinear dynamic analysis. There are two types of analysis concerning the software's used; coupled or uncoupled analysis. The uncouple analysis calculates blast loads as if the structure (and its components) were rigid and then applying these loads to responding model of the structure. The shortcoming of this procedure is that when the blast field is obtained with a rigid model of the structure, the loads on the structure are often over-predicted, particularly if significant motion or failure of the structure occurs during the loading period.

For a coupled analysis, the blast simulation module is linked with the structural response module. In this type of analysis, the CFD (computational fluid mechanics) model for blast-load prediction is solved simultaneously with the CSM (computational solid mechanics) model for structural response. By accounting for the motion of the structure while the blast calculation proceeds, the pressures that arise due to motion and failure of the structure can be predicted more accurately. In this type of analysis Considerable skill is required to evaluate the output of the computer code, both as to its correctness and its appropriateness to the situation modelled; without such judgment, it is possible through a combination of modelling errors and poor interpretation to obtain erroneous or meaningless results. Therefore, successful computational modelling of specific blast scenarios by engineers unfamiliar with these programs is difficult [27].In this thesis uncoupled analysis commercially available finite element structural software is used i.e. SAP2000 to perform linear dynamic analysis.

# CHAPTER 4 CASE STUDY ON REINFORCED CONCRETE FRAME BUILDING SUBJECTED TO SUB SURFACE EXPLOSSION AND EARTH QUAKE LOADING.

## 4.1 Introduction

This chapter illustrates a theoretical study that was carried out on reinforced concrete frame building subjected to sub surface blast loads and earth quake loads. First, the building is designed for dead, live, and earthquake loads according to the specification of ES EN1998-1, 2015 (EBCS) guidelines. Then the structure was subjected to sub surface blast loads resulting from detonation of an equivalent (3kg of TNT) weight at different depth of burial (standoff distances) and analyzed using SAP 2000 software and responses are obtained. Then the same model but without dynamic increase factor is analyzed for an earthquake motion characterized by the elastic design spectrum (Type 1 and 2) of ES EN1998-1, 2015 scaled to different peak ground acceleration and 5% damping and the responses are compared with the responses of the building for sub surface blast loads of different cases. Finally, equivalent seismic loads are established for the sub surface blast loads of different cases.

## 4.2 Preliminary design

In this chapter, a description of the configuration of the study buildings, Member sizes and material properties used in the design are described. It also defines the seismic loading parameters and capacity design principles according to ES EN 1998-2, 2015.

### 4.2.1 Modelling

In this section, models of the building are created using sap 2000 structural analysis and design software. For modelling the frames, the first trial minimum section sizes are used which fulfils the minimum geometric requirements of ES EN: 1998-1, 2015 for medium ductility. A total of four (4) building models are analyzed and designed for preliminary design assuming ground acceleration of 0.2g in soil type D, spectrum type 2 and 5% damping. The investigated building is a multi-story reinforced concrete structure. The elevation of the building and

floor plans (typical) are shown in Figs (4.2&4.3). The buildings has 6 and 12 story and with number of bays of 3 by 3 and 3 by 4 for each story. The width of the bays considered are 4m in both direction (X and Y). The total height of the building above the ground is 18 m for 6 story and 36 m for 12 story. The height of the story of both buildings amounts to 3 m. The reason for keeping bay width and story height dimension constant is to remove the effects of the variations of this parameters in analysis. The structural system consists of frames. Poisson's ratio was taken equal to c = 0 (cracked concrete) [29] and Steel S4000 Class C is used. The structure will be designed for ductility class DCM.

The structure was assumed to have the following properties:

1. All connections were assumed to be moment resistance.

2. Column to foundation connections are considered fixed.

3. Material properties: concrete strength (f'c) = 30 MPa, rebar yield strength (fy) = 400 MPa. Modulus of elasticity of concrete (Ec) = 31 GPa and modulus of elasticity of rebar (Es) = 200 GPa.

Then after performing preliminary design, the common section size and reinforcement requirement which is safe for both number of bays (3x3 and 3x4) are selected for each story. After selecting section size and reinforcement requirements total of twelve (12) buildings are modelled for the completion of the objectives of this research. The data necessary to analyze the models are summarized below. All the models selected are regular in plan and elevation as shown in figs (4.2 &4.3)

For the seismic design situation, it is necessary to adjust the size /stiffness of earthquake-resistant elements according to the value of the seismic action corresponding to each ductility demand with the aim of verifying the relevant limit states. So, in this context, to all models, it was done an iterative process to obtain the final structural definition.

### 4.2.2 Loads and Load Combinations

In this research the loads applied on the structures for preliminary design are dead load, live load and seismic loads. The load combinations are created as per (ES EN 1998: -2015). A total of 34 load combinations are considered for all models and the maximum action effects are used for analysis and design of the buildings. The dead loads considered in this project are the self-weight of the structure and additional dead load of 2.5kN/$m^2$ to consider floor finish and partition wall loads. The live load is taken from the structural function of the buildings and is chosen as 2.5 kN/$m^2$ assuming the floor is used for office rooms in hospitals and business buildings with separate store.

### 4.2.3 Behavior Factor

For purposes of defining the value of behavior coefficient, it is necessary to classify the structural system and define their regularity in plan and height. If the structure is not defined by regular in height, the reference values of behavior coefficient must be reduced by 20%. The lateral force resisting mechanism of the models used in this research is frame system thus, the values of q calculated according to ES EN 1998-1,2015 section 5.2.2.2 is used for analysis. The energy dissipation capacity of the structure is considered mainly through the ductile behavior of its elements by performing a linear analysis based on a reduced response spectrum, called design spectrum. This reduction is accomplished by introducing the behavior factor q.

The value of behavior factor is defined by the following equation.

$$q = q_o . k_w \quad (4.1)$$

Where;

- $q_o$ is the basic value of the behavior factor, dependent on the type of the structural system and on its regularity in elevation
- $k_w$ is the factor reflecting the prevailing failure mode in structural systems with walls.

For Frame system regular in elevation, the values of $q_0$ is calculate as;

$$q_0 = 3\frac{\alpha_u}{\alpha_1} \quad (4.2)$$

Where:

- $\alpha_1$ is the value by which the horizontal seismic design action is multiplied in order to first reach the flexural resistance in any member in the structure, while all other design actions remain constant;
- $\alpha_u$ is the value by which the horizontal seismic design action is multiplied, in order to form plastic hinges in a number of sections sufficient for the development of overall structural instability, while all other design actions remain constant.

According to ES EN 1998-1, 2015, for multi-story, multi-bay frames or frame-equivalent dual structures which is regular in elevation: $\alpha_u/\alpha_1$ =1.3. Therefore; the values of behavior factor is q=3x1.3=3.9

### 4.2.4 Analysis Verification and 2nd Order Effects

The application of ES EN: 1998-2015 on design of structures subjected to seismic action is intended to ensure three objectives:

1) Safeguarding human lives;

2) limit structural damage;

3) Important structures for civil protection remain operational.

In this context, it is necessary that structures are designed for non-occurrence of local or global collapse to a seismic level with small probability of occurrence, designated as design seismic action, and is controlled the damage level in the same structure for a seismic action with minor intensity and higher probability of occurrence than the design seismic action. The damage should not correspond to disproportionately high costs when compared to the structure itself. These two requirements are accomplished, if the two limit states are verified:

**1. Ultimate limit states:** For ultimate limit states verifications, Inter-story drift sensitivity coefficient should be evaluated as follows.

If $\theta \leq 0.10$ second order effects can be ignored otherwise 2nd order effects have to be considered. But the value of the coefficient θ shall not exceed 0.3.

$$\theta = \frac{P_{tot}.d_r}{V_{tot}.h} \leq 0.1 \quad (4.3)$$

Where;

- θ = Inter-story drift sensitivity coefficient
- $P_{tot}$ = total gravity load at and above the story considered in the seismic design situation
- $V_{tot}$ = total seismic story shear at and above the story considered
- h = inter-story height
- $d_r$ = design inter-story drift, evaluated as the difference of the average lateral displacement's

**2. Damage limit state:** The "damage limitation requirement" is considered to be satisfied, if drift limits according to the following expressions are satisfied (ES EN 1998-1, 2015).

a) $d_r v \leq 0.005h$ ; for a structure having non-structural element with brittle materials.

b) $d_r v \leq 0.0075h$; for a structure having ductile non-structural element.

c) $d_r v \leq 0.010h$; for a structure without non-structural elements.

v is the reduction coefficient whose value is 0.4 for importance class IV and V and 0.5 for important class I and II

In this thesis the investigated building is considered as ordinary buildings which belongs to importance class of II.

### 4.2.5 Analysis of Buildings

After modelling and performing the preliminary design of the structure to the vertical loads, response spectrum analysis is performed for all the models described in the previous sections.

After performing linear elastic analysis, the corresponding ultimate and damage limit state requirements of the code are checked and respected.

The size / stiffness of the elements was obtained by a process of iteration as the demand of the ductility classes for each model and optimized sections are obtained keeping the satisfaction of the limits provided in the design codes. In all cases, the sections are selected to full fill all the capacity design requirements.

As a design tool, the capacity design approach is widely recognized in the field of earthquake engineering. Resulting from nonlinear response and energy absorption ability (R > 1.5), structures subjected to linear analyses with reduced seismic design forces require use of the capacity design approach.

The aim of capacity design is to control the inelastic seismic response. (M.N. Fardis, 2009[29]) states that Capacity design can be achieved through;

1. Structural configuration and relative sizing of members to ensure a beam-sway mechanism,

2. Detailing of plastic hinge regions (beam ends, base of columns and walls) to sustain inelastic deformation demands. Plastic hinge regions are detailed for deformation (ductility) demands.

In capacity design of buildings;

- Avoid weak column / strong beam frames
- Avoid Soft-story collapse mechanism through proper structural configuration

Provide strong column/weak beam frames, with beam sway mechanisms, involves plastic hinging at all beam ends either plastic hinging at column bottoms, or rotations at the foundation.

In capacity design the fulfilment of strong column/weak beam capacity design rule is maintained with over strength factor $\gamma_{Rd}$ on beam strengths. Sum of column resistances is > 1.3 of sum of beam resistances for each node.

$$\sum M_{RC} \geq \gamma_{RD} \sum M_{RB} \quad (4.4)$$

The recommended value for the over strength factor in the code is $\gamma_{RD}$ =1.3 for frames and frame equivalent dual system.

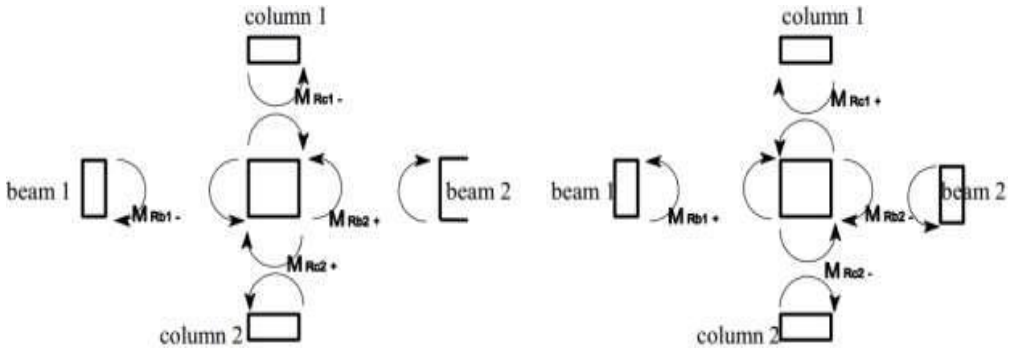


**Figure 4.1: Beam and column flexural capacity at a joint in capacity design rule (M.N. Fardis, 2009 [30]).**

### 4.2.6 Design Action Effects

The design values of bending moments and axial forces are obtained from the analysis of the structure for the seismic design situation by considering second order effects when it was found necessary. The design values of shear forces of primary seismic beams and columns are determined as follows.

**1. Beams**

The design shear forces for beams are determined in accordance with the capacity design rule considering;

a) The transverse load acting on it in the seismic design situation and

b) End moments $M_{i,d}$ (with i=1,2 denoting the end sections of the beam), corresponding to plastic hinge formation for positive and negative directions of seismic loading. The plastic hinges should be taken to form at the ends of the beams or (if they form there first) in the vertical elements connected to the joints into which the beam ends frame.

$$M_{i,d} = \gamma_{RD} * M_{Rb,I} * \min\left(1, \frac{\sum M_{rc}}{\sum Mrb}\right) \quad (4.5)$$

Where;

- $\gamma_{RD}$ is the factor accounting for possible over strength due to steel strain hardening, which in the case of DCM beams may be taken as being equal to 1.0;
- $M_{Rb,I}$ is the design value of the beam moment of resistance at end i in the sense of the seismic bending moment under the considered sense of the seismic action;
- $\Sigma M_{Rc}$ and $\Sigma M_{Rb}$ are the sum of the design values of the moments of resistance of the columns and the sum of the design values of the moments of resistance of the beams framing into the joint, respectively.

The value of $\Sigma M_{Rc}$ should correspond to the column axial force(s) in the seismic design situation for the considered sense of the seismic action.

**2. Columns**

In primary seismic columns the design values of shear forces shall be determined in accordance with the capacity design rule, on the basis of the equilibrium of the column under end moments $M_{i,d}$ (with i=1,2 denoting the end sections of the column), corresponding to plastic hinge formation for positive and negative directions of seismic loading. The plastic hinges should be taken to form at the ends of the beams connected to the joints into which the column end frames, or (if they form there first) in the columns. End moments $M_{i,d}$ may be determined from the following expression:

$$M_{i,d} = \gamma_{RD} * M_{Rc,I} * \min\left(1, \frac{\sum M_{rb}}{\sum M_{rc}}\right) \quad (4.6)$$

Where;

- $\gamma_{RD}$ is the factor accounting for over strength due to steel strain hardening and confinement of the concrete of the compression zone of the section, taken as being equal to 1.1 for DCM;

- $M_{Rc,i}$ is the design value of the column moment of resistance at end i in the sense of the seismic bending moment under the considered sense of the seismic action;
- $\Sigma M_{Rc}$ and $\Sigma M_{Rb}$ are as defined above.

To ensure local and global ductility of the structure, (ES EN 1998:1-2015) considers the following calculation rules for real capacity. It should be prevented the formation of brittle failure mechanisms or mechanisms undesirable, such as shear failure of resistant elements or concentration of plastic hinges in columns of a single story. To this end, design values should be obtained by equilibrium conditions considering resistant values at adjacent sections and a $\gamma_{RD}$ factor whose value varies from element to element and the ductility class of the structure. Eq. (4.7) should be checked for all nodes between primary or secondary beams and primary columns of frame systems or frame equivalent systems with two or more floors.

$$\sum M_{RC} \geq 1.3 \sum M_{RB} \tag{4.7}$$

Where;

- $\Sigma M_{RC}$; sum of resistant bending moments of columns connected to node.
- $\Sigma M_{RB}$; sum of resistant bending moments of beams connected to node.

After performing preliminary design, geometric and Structural details of the models are presented in tables 4.1-4.2 and Figs 4.2-4.3.

**Table 4.1:Description of the model.**

| Number of bay | | Width of bay in both direction/m | Number of story | Height of story/m |
|---|---|---|---|---|
| In x-direction | In y-direction | | | |
| 3 | 3 | 4 | 6 | 3 |
| | | 4 | 12 | 3 |
| 3 | 4 | 4 | 6 | 3 |
| | | 4 | 12 | 3 |

**Table 4.2:Description of structural elements.**

| Number of bay | | Number of story | Section group | Section size/m | Reinforcement area/mm$^2$ | |
|---|---|---|---|---|---|---|
| In x-direction | In y-direction | | | | Top | Bottom |
| 3 | 3 | 6 | Beam | 0.4x0.3 | 1097 | 622 |
| 3 | 4 | | Column | 0.5x0.5 | 2248.24 | |
| 3 | 3 | 12 | Beam | 0.4x0.3 | 1205 | 602.88 |
| 3 | 4 | | Column | 0.6x0.6 | 3768 | |

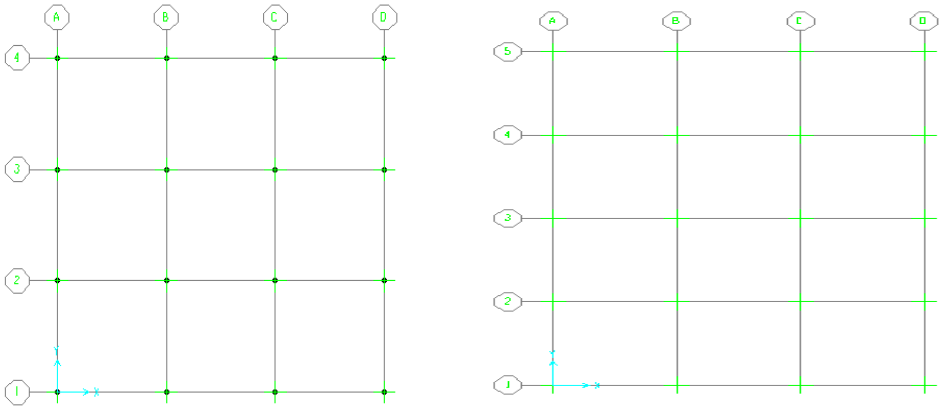

**Figure 4.2:Floor plans of (3x3) and (3x4) bay frame structure for both 6 and 12 story.**

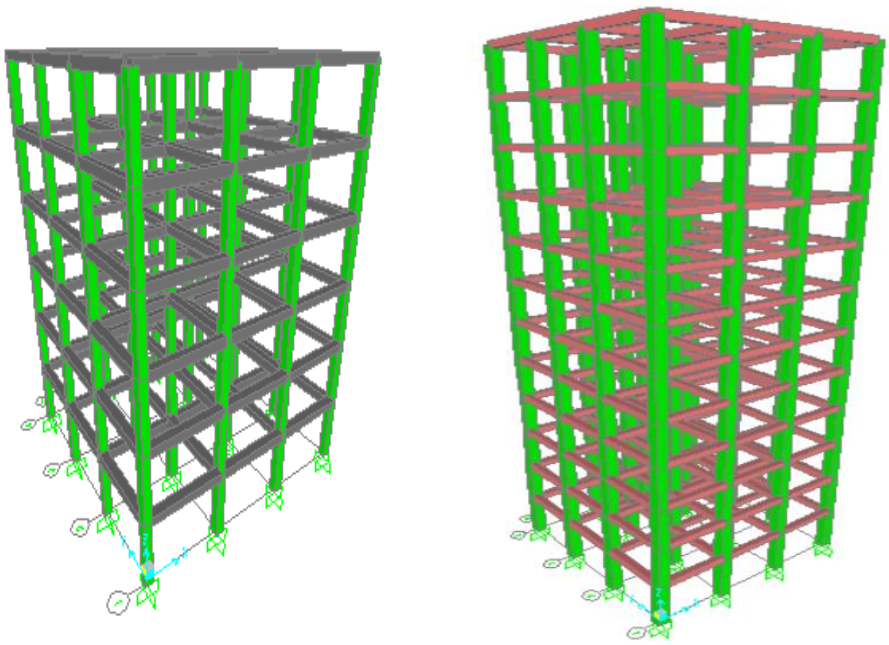

**Figure 4.3:Elevation views of both 6-story and 12-story frame structures for both (3x3) and (3x4) bays.**

## 4.3 Analysis of building model using linear dynamic procedure for sub surface blast loads

In this section the building is analyzed using three dimensional analysis program (SAP2000). If only elastic material behavior is considered, linear analysis method should suffice, though P-delta formulations may still be applied. Therefore the building first analyzed using nonlinear static case as an initial state, since it is often necessary to start from a nonlinear static state to consider geometric non linearity in model [9]. Then the building is analyzed using linear direct integration time history analysis during sub surface explosion events.

### 4.3.1 Modeling and assumption

The linear dynamic analysis is done by a step-by-step integration of the equilibrium equations in the time domain. Standard direct integration methods available in SAP 2000 was executed. Newmark's method of numerical integration was used with gamma = 0.5 and beta = 0.25. This values of gamma and beta are satisfactory from all points of view including that of convergence and accuracy [5]. With these parameters, the method is equivalent to the average acceleration method. Geometric nonlinearity and the effect of large deformations is accounted for in the models, by considering P-delta effects. This can be performed on sap 2000 by allowing the linear time history analysis to use stiffness at the end of nonlinear case 'P-delta'. Mass and stiffness proportional damping (Rayleigh damping) was used to damp both high and low frequency modes outside of the range significant to dynamic response. The range of important times were identified during the modal analysis and was used to SAP2000 to calculate Rayleigh damping coefficients. These coefficients were then used throughout the time history analyses. The maximum time step used was 0.002sec for all cases.

## 4.4 Analysis of building model using linear elastic structural analysis (response spectrum analysis) procedure for earth quake loads.

For earth quake analysis an earthquake motion characterized by the elastic design spectrum (Type 1 and 2) of ES EN1998-1, 2015 [4] scaled to different peak ground acceleration and 5% damping are considered for different soil class. Site specific

response spectrum curves (elastic and design) are generated for different scaled peak ground acceleration [20] and different ground type in both spectrum (1 and 2) according to ES EN 1998-1, 2015. Then this response spectrum curves are used in sap 2000 for analysis of target structure. The procedures followed and generated response spectrum curves are presented in appendix A

### 4.4.1 Modeling and assumption

For seismic analysis of the building, a 3D model of the building is used, where an earthquake motion characterized by the elastic design spectrum (Type 1 and 2) of ES EN 1998-1, 2015 scaled to different peak ground acceleration and in different ground types are applied to the structure in the same horizontal direction as the applied blast loads. Then the building is analyzed using sap 2000 software by response spectrum analysis procedure. Response spectrum analysis is done using response spectrum curves for different spectrum and ground types using 5 % damping which is generated according to guide lines of ES EN1998-1, 2015 and behavior factor q of 1. In the seismic analysis, no strength or dynamic increase factors are used. However, the same material models for concrete and steel reinforcement as used in the blast analysis are utilized.

## 4.5 Results and discussion

### 4.5.1 Responses of a structure for Blast load

Tables 4.3 to 4.6 list the floor displacements and story drifts of the 6-story and 12-story frame structures under the action of an equivalent 3kg of TNT sub surface explosion per blasting field, their distances from the explosion source are 4 m, 7 m and 10 m.

**Table 4.3:Floor displacements of 6-story 3-bay by 3-bay frame structure subjected to sub surface explosion of equivalent 3kg of TNT.**

| Story | Stand of distance (m) | | | | | |
|---|---|---|---|---|---|---|
| | 4m | | 7m | | 10m | |
| | Floor displacement (m) | Story drift (m) | Floor displacement (m) | Story drift (m) | Floor displacement (m) | Story drift (m) |
| 1 | 0.0044 | 0.0044 | 0.0016 | 0.0016 | 0.0007 | 0.0007 |
| 2 | 0.0135 | 0.0091 | 0.0037 | 0.0021 | 0.0016 | 0.0009 |

| | | | | | | |
|---|---|---|---|---|---|---|
| 3 | 0.0199 | 0.0064 | 0.0056 | 0.0019 | 0.0024 | 0.0008 |
| 4 | 0.0237 | 0.0038 | 0.0068 | 0.0012 | 0.0030 | 0.0006 |
| 5 | 0.0274 | 0.0037 | 0.0079 | 0.0011 | 0.0034 | 0.0004 |
| 6 | 0.0318 | 0.0044 | 0.0089 | 0.0010 | 0.0039 | 0.0005 |

**Table 4.4:Floor displacements of 12-story 3-bay by 3-bay frame structure for sub surface explosion of equivalent 3kg of TNT.**

| Story | Stand of distance (m) | | | | | |
|---|---|---|---|---|---|---|
| | 4m | | 7m | | 10m | |
| | Floor displacement (m) | Story drift (m) | Floor displacement (m) | Story drift (m) | Floor displacement (m) | Story drift (m) |
| 1 | 0.0034 | 0.0034 | 0.0012 | 0.0012 | 0.0006 | 0.0006 |
| 2 | 0.0108 | 0.0074 | 0.0032 | 0.0020 | 0.0015 | 0.0009 |
| 3 | 0.0193 | 0.0085 | 0.0055 | 0.0023 | 0.0025 | 0.001 |
| 4 | 0.0265 | 0.0072 | 0.0073 | 0.0018 | 0.0032 | 0.0007 |
| 5 | 0.0324 | 0.0059 | 0.0089 | 0.0016 | 0.0041 | 0.0009 |
| 6 | 0.0351 | 0.0027 | 0.0097 | 0.0008 | 0.0048 | 0.0007 |
| 7 | 0.0397 | 0.0046 | 0.0111 | 0.0014 | 0.0054 | 0.0006 |
| 8 | 0.0468 | 0.0071 | 0.0131 | 0.002 | 0.0059 | 0.0005 |
| 9 | 0.0529 | 0.0061 | 0.0149 | 0.0018 | 0.0065 | 0.0006 |
| 10 | 0.0571 | 0.0042 | 0.0161 | 0.0012 | 0.0071 | 0.0006 |
| 11 | 0.0622 | 0.0051 | 0.0176 | 0.0015 | 0.0077 | 0.0006 |
| 12 | 0.0661 | 0.0039 | 0.0187 | 0.0011 | 0.0081 | 0.0004 |

**Table 4.5: Floor displacements of 6-story 3-bay by 4-bay frame structure for sub surface explosion of equivalent 3kg of TNT.**

| Story | Stand of distance (m) | | | | | |
|---|---|---|---|---|---|---|
| | 4m | | 7m | | 10m | |
| | Floor displacement (m) | Story drift (m) | Floor displacement (m) | Story drift (m) | Floor displacement (m) | Story drift (m) |
| 1 | 0.0081 | 0.0081 | 0.0023 | 0.0023 | 0.001 | 0.001 |
| 2 | 0.0081 | 0 | 0.0023 | 0 | 0.001 | 0 |
| 3 | 0.0081 | 0 | 0.0023 | 0 | 0.001 | 0 |
| 4 | 0.0081 | 0 | 0.0023 | 0 | 0.001 | 0 |
| 5 | 0.0081 | 0 | 0.0023 | 0 | 0.001 | 0 |
| 6 | 0.0146 | 0.0065 | 0.003 | 0.0007 | 0.0013 | 0.0003 |

**Table 4.6: Floor displacements of 12-story 3-bay by 4-bay frame structure for sub surface explosion of equivalent 3kg of TNT.**

| Story | Stand of distance (m) | | | | | |
|---|---|---|---|---|---|---|
| | 4m | | 7m | | 10m | |
| | Floor displacement (m) | Story drift (m) | Floor displacement (m) | Story drift (m) | Floor displacement (m) | Story drift (m) |
| 1 | 0.0095 | 0.0095 | 0.0026 | 0.0026 | 0.001 | 0.001 |
| 2 | 0.0195 | 0.01 | 0.0056 | 0.003 | 0.0023 | 0.0013 |
| 3 | 0.0197 | 0.0002 | 0.0056 | 0 | 0.0023 | 0 |
| 4 | 0.0199 | 0.0002 | 0.0056 | 0 | 0.0023 | 0 |
| 5 | 0.02 | 1E-04 | 0.0056 | 0 | 0.0023 | 0 |
| 6 | 0.025 | 0.005 | 0.007 | 0.0014 | 0.0029 | 0.0006 |
| 7 | 0.0307 | 0.0057 | 0.0087 | 0.0017 | 0.0037 | 0.0008 |
| 8 | 0.0359 | 0.0052 | 0.01 | 0.0013 | 0.0043 | 0.0006 |
| 9 | 0.0402 | 0.0043 | 0.0115 | 0.0015 | 0.005 | 0.0007 |
| 10 | 0.0487 | 0.0085 | 0.0139 | 0.0024 | 0.0061 | 0.0011 |
| 11 | 0.0553 | 0.0066 | 0.0159 | 0.0020 | 0.0070 | 0.0009 |
| 12 | 0.0617 | 0.0064 | 0.0177 | 0.0018 | 0.0077 | 0.0007 |

From Tables 4.3 to 4.6, the maximum floor displacements of 6-story and 12-story frame structures can be obtained and the results are shown in Fig (4.4).

According to Tables 4.3, 4.4, 4.5 and 4.6, the vibration response of the top story is maximum under the action of blasting wave. Fig (4.4) shows that with the increase of the explosion distance, the blasting vibration response decreases.

From Tables 4.3, 4.4, 4.5 and 4.6, the biggest story drift of 6-story 3-Bay by 3-Bay frame structure appears on second story under the action of 4 m, 7 m and 10 m explosion distance; and the biggest story drift of 12-story 3-Bay by 3-Bay frame structure appears on the third story under the action of 4 m, 7 m and 10 m explosion distances. But for 3-Bay by 4-Bay frame structure the biggest story drift of 6-story frame structure, all appear on first story under the action of 4 m,7 m and 10 m explosion distance; and the biggest story drift of 12-story all appear on second story under the action of 4 m,7 m and 10 m.

The above discussion indicates that maximum story drifts of all above cases appears at lower story indicating that much of energy which comes from subsurface blast loads to the structure is dissipated by lower story.

The maximum story drifts of 6-story and 12-story frame structures are shown in (Fig 4.5).

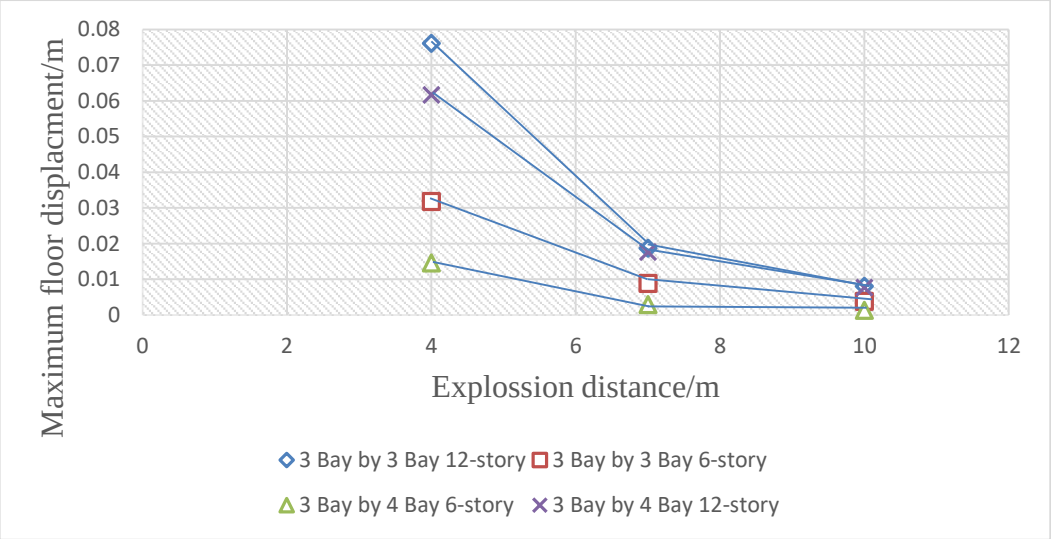


**Figure 4.4: Maximum floor displacement of frame structures.**

From Fig (4.5), the story drifts of 6-story and 12-story frame structures are maximum under the action of 4 m explosion distance. With the increase of explosion distance, the story drifts gradually reduce. At the distance of 4 m when the number of bays is 3 by 3, the maximum story drifts of 6-story is 0.0091 but when the number of bays is 3 by 4, the maximum story drift is 0.0081. For 12-story when the number of bays is 3 by 3, the maximum story drift is 0.0085 but when the number of bays is 3 by 4, the maximum story drift is 0.01. While at the distance of 7 m and 10 m and for both 6 and 12-story the maximum story drifts are almost the same for both 3 by 3 Bay and 3 by 4 Bay frame structure. The above discussion indicates that the number of bays of the structure has a greater impact on the story drifts when the explosion distance is small but with different effects on lower and higher structure. For lower structure the maximum story drift decreases with increase of number of bays of a structure. In contrary, for higher structure the maximum story drift increases with increase of number of bays of the structure.

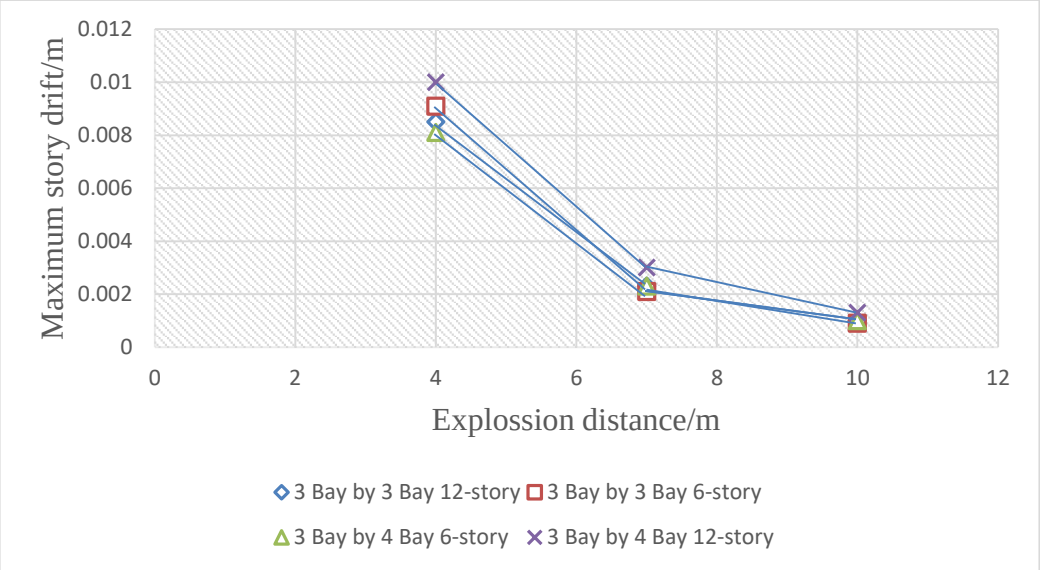


**Figure 4.5:Maximum story drift of frame structure.**

As can be seen from Figs (4.4 and 4.5), under the same explosion source distance, the lower the number of the bays of structure, the greater the maximum displacement of the floor. The maximum floor displacement and maximum story drift caused by blasting vibration are all weakened with increase of explosion source distance. The floor displacements of both 6-story and 12- story RC frame structure all have decreased trend between 7m and 10m stand of distance indicating that the change rate of floor displacement is smaller when explosion distance is farther.

### 4.5.2 Responses of a structure for earth quake loadings.

Tables 4.7 to 4.10 lists the maximum floor displacements of the 6-story and 12-story frame structures subjected to an earthquake motion characterized by the elastic design spectrum (Type 1 and 2) of ES EN1998-1, 2015 scaled to different peak ground acceleration and different ground types.

**Table 4.7: Maximum top story displacements of (3x3) Bay 6-story frame structure for spectrum type 1.**

| Peak ground acceleration in g | Spectrum type 1 | | | |
|---|---|---|---|---|
| | Ground types | | | |
| | A | B | C | D |
| 0.05 | 0.0043 | 0.0059 | 0.0043 | 0.0950 |
| 0.06 | 0.0052 | 0.0071 | 0.0052 | 0.0114 |
| 0.07 | 0.0061 | 0.0082 | 0.0061 | 0.0132 |

| | | | | |
|---|---|---|---|---|
| 0.08 | 0.0070 | 0.0094 | 0.0070 | 0.0151 |
| 0.09 | 0.0078 | 0.0106 | 0.0079 | 0.0170 |
| 0.1 | 0.0087 | 0.0118 | 0.0087 | 0.0189 |
| 0.2 | 0.0175 | 0.0236 | 0.0175 | 0.0378 |
| 0.3 | 0.0263 | 0.0355 | 0.0263 | 0.0568 |
| 0.4 | 0.0344 | 0.0464 | 0.0351 | 0.0757 |
| 0.5 | 0.0438 | 0.0591 | 0.0439 | 0.0946 |
| 0.6 | 0.0526 | 0.0710 | 0.0527 | 0.1135 |
| 0.7 | 0.0602 | 0.0828 | 0.0615 | 0.1324 |
| 0.8 | 0.0701 | 0.0946 | 0.0702 | 0.1513 |
| 0.9 | 0.0789 | 0.0145 | 0.0790 | 0.1703 |
| 1 | 0.0876 | 0.1183 | 0.0870 | 0.1892 |
| 1.1 | 0.0946 | 0.1301 | 0.0966 | 0.2081 |
| 1.2 | 0.1052 | 0.1420 | 0.1054 | 0.2270 |
| 1.3 | 0.1139 | 0.1538 | 0.1142 | 0.2459 |
| 1.4 | 0.1227 | 0.1657 | 0.1230 | 0.2649 |
| 1.5 | 0.1315 | 0.1775 | 0.1318 | 0.2838 |
| 1.6 | 0.1402 | 0.1893 | 0.1405 | 0.3027 |
| 1.7 | 0.1463 | 0.2012 | 0.1493 | 0.3216 |
| 1.8 | 0.1578 | 0.2091 | 0.1581 | 0.3405 |
| 1.9 | 0.1635 | 0.2248 | 0.1669 | 0.3595 |
| 2 | 0.1753 | 0.2367 | 0.1757 | 0.3784 |

**Table 4.8:Maximum top story displacements of (3x3) Bay 6-story frame structure for spectrum type 2**

| Peak ground acceleration in g | Spectrum type 2 | | | |
|---|---|---|---|---|
| | Ground types | | | |
| | A | B | C | D |
| 0.05 | 0.0070 | 0.0085 | 0.0085 | 0.0100 |
| 0.06 | 0.0084 | 0.0101 | 0.0102 | 0.0120 |
| 0.07 | 0.0098 | 0.0118 | 0.0120 | 0.0140 |
| 0.08 | 0.0112 | 0.0135 | 0.0137 | 0.0160 |
| 0.09 | 0.0126 | 0.0152 | 0.0154 | 0.0180 |
| 0.1 | 0.0140 | 0.0169 | 0.0171 | 0.0200 |
| 0.2 | 0.0280 | 0.0338 | 0.0342 | 0.0401 |
| 0.3 | 0.04200 | 0.0507 | 0.0512 | 0.0601 |
| 0.4 | 0.0560 | 0.0657 | 0.0683 | 0.0802 |
| 0.5 | 0.0700 | 0.0845 | 0.0854 | 0.1002 |
| 0.6 | 0.0840 | 0.1014 | 0.1025 | 0.1203 |
| 0.7 | 0.0980 | 0.1184 | 0.1196 | 0.1403 |
| 0.8 | 0.1120 | 0.1359 | 0.1366 | 0.1604 |
| 0.9 | 0.1260 | 0.1478 | 0.1537 | 0.1804 |

| | | | | |
|---|---|---|---|---|
| 1 | 0.1400 | 0.1691 | 0.1708 | 0.2005 |
| 1.1 | 0.1541 | 0.1860 | 0.1879 | 0.2205 |
| 1.2 | 0.1681 | 0.2029 | 0.2049 | 0.2406 |
| 1.3 | 0.1821 | 0.2198 | 0.2220 | 0.2606 |
| 1.4 | 0.1961 | 0.2367 | 0.2391 | 0.2807 |
| 1.5 | 0.2101 | 0.2536 | 0.2562 | 0.3007 |
| 1.6 | 0.2241 | 0.2705 | 0.2733 | 0.3208 |
| 1.7 | 0.2381 | 0.2792 | 0.2903 | 0.3408 |
| 1.8 | 0.2521 | 0.3043 | 0.3074 | 0.3609 |
| 1.9 | 0.2661 | 0.3212 | 0.3245 | 0.3809 |
| 2 | 0.2801 | 0.3382 | 0.3416 | 0.3906 |

**Table 4.9:Maximum top story displacements of (3x3) Bay 12-story frame structure for spectrum type 1**

| Peak ground acceleration in g | Spectrum type 1 | | | |
|---|---|---|---|---|
| | Ground types | | | |
| | A | B | C | D |
| 0.05 | 0.0096 | 0.0129 | 0.0096 | 0.0207 |
| 0.06 | 0.0115 | 0.0155 | 0.0115 | 0.0248 |
| 0.07 | 0.0134 | 0.0181 | 0.0315 | 0.0289 |
| 0.08 | 0.0153 | 0.0207 | 0.0154 | 0.033 |
| 0.09 | 0.0172 | 0.0232 | 0.0173 | 0.0372 |
| 0.1 | 0.0191 | 0.0258 | 0.0192 | 0.0413 |
| 0.2 | 0.0383 | 0.0516 | 0.0385 | 0.0826 |
| 0.3 | 0.0574 | 0.0775 | 0.0577 | 0.1239 |
| 0.4 | 0.0755 | 0.102 | 0.077 | 0.1652 |
| 0.5 | 0.0956 | 0.1291 | 0.0962 | 0.2065 |
| 0.6 | 0.1148 | 0.1549 | 0.1154 | 0.2479 |
| 0.7 | 0.1322 | 0.1808 | 0.1347 | 0.2892 |
| 0.8 | 0.153 | 0.2066 | 0.1539 | 0.3305 |
| 0.9 | 0.1722 | 0.2294 | 0.1731 | 0.3718 |
| 1 | 0.1913 | 0.2582 | 0.1924 | 0.4131 |
| 1.1 | 0.2077 | 0.2841 | 0.2116 | 0.4544 |
| 1.2 | 0.2295 | 0.3099 | 0.2309 | 0.4957 |
| 1.3 | 0.2485 | 0.3357 | 0.2501 | 0.537 |
| 1.4 | 0.2678 | 0.3615 | 0.2693 | 0.5783 |
| 1.5 | 0.2869 | 0.3871 | 0.2886 | 0.6196 |
| 1.6 | 0.3058 | 0.4132 | 0.3075 | 0.6609 |
| 1.7 | 0.321 | 0.439 | 0.327 | 0.7023 |
| 1.8 | 0.3443 | 0.4588 | 0.3463 | 0.7436 |
| 1.9 | 0.3588 | 0.4906 | 0.3655 | 0.7849 |
| 2 | 0.3826 | 0.5165 | 0.3848 | 0.8262 |

**Table 4.10:Maximum top story displacements of (3x3) Bay 12-story frame structure for spectrum type 2.**

| Peak ground acceleration in g | Spectrum type 2 | | | |
|---|---|---|---|---|
| | Ground types | | | |
| | A | B | C | D |
| 0.05 | 0.0153 | 0.0229 | 0.0263 | 0.0411 |
| 0.06 | 0.0183 | 0.0274 | 0.0315 | 0.0493 |
| 0.07 | 0.0214 | 0.032 | 0.0368 | 0.0575 |
| 0.08 | 0.0244 | 0.0366 | 0.042 | 0.0657 |
| 0.09 | 0.0275 | 0.0411 | 0.0473 | 0.0739 |
| 0.1 | 0.0305 | 0.0457 | 0.0525 | 0.0821 |
| 0.2 | 0.061 | 0.0914 | 0.105 | 0.1642 |
| 0.3 | 0.0915 | 0.1371 | 0.1575 | 0.2464 |
| 0.4 | 0.122 | 0.1803 | 0.2101 | 0.3286 |
| 0.5 | 0.1525 | 0.2285 | 0.2626 | 0.4107 |
| 0.6 | 0.1831 | 0.2742 | 0.3151 | 0.4928 |
| 0.7 | 0.2136 | 0.3199 | 0.3676 | 0.575 |
| 0.8 | 0.2441 | 0.3655 | 0.4202 | 0.6571 |
| 0.9 | 0.2746 | 0.4056 | 0.4726 | 0.7392 |
| 1 | 0.3051 | 0.457 | 0.5252 | 0.8214 |
| 1.1 | 0.3356 | 0.5027 | 0.5777 | 0.9035 |
| 1.2 | 0.3661 | 0.5484 | 0.6302 | 0.9857 |
| 1.3 | 0.3966 | 0.5941 | 0.6847 | 1.0678 |
| 1.4 | 0.4271 | 0.6398 | 0.7352 | 1.1499 |
| 1.5 | 0.4576 | 0.6855 | 0.7877 | 1.2321 |
| 1.6 | 0.4881 | 0.7312 | 0.8403 | 1.3142 |
| 1.7 | 0.5187 | 0.7661 | 0.8928 | 1.3964 |
| 1.8 | 0.5492 | 0.8226 | 0.9453 | 1.4785 |
| 1.9 | 0.5797 | 0.8683 | 0.9978 | 1.5606 |
| 2 | 0.6102 | 0.914 | 1.0503 | 1.6202 |

According to Tables 4.7, 4.8, 4.9 and 4.10, the vibration response of the top story is maximum under the action of earth quake loads. Fig (4.6) and Fig (4.7) shows that with the increase of peak ground acceleration, vibration response increases for all ground types.

From the Tables 4.7, 4.8, 4.9 and 4.10, for spectrum type 1, biggest to smallest top story displacement of both 6-story and 12-story frame structure was found when the structure is analysed for ground types of D, B, C and A respectively.But for spectrum type 2 biggest to smallest top story displacement of both 6-story and 12-story frame structure was found when the structure is analysed for ground types of D, C, B and A respectively.

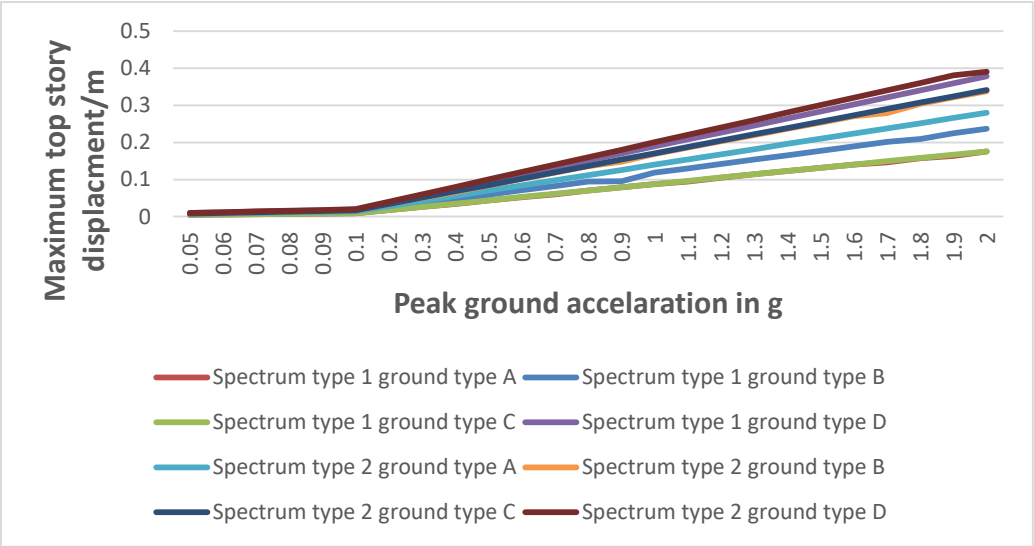


**Figure 4.6 : Maximum top story displacements of 6-story frame structures subjected to an earthquake motion.**

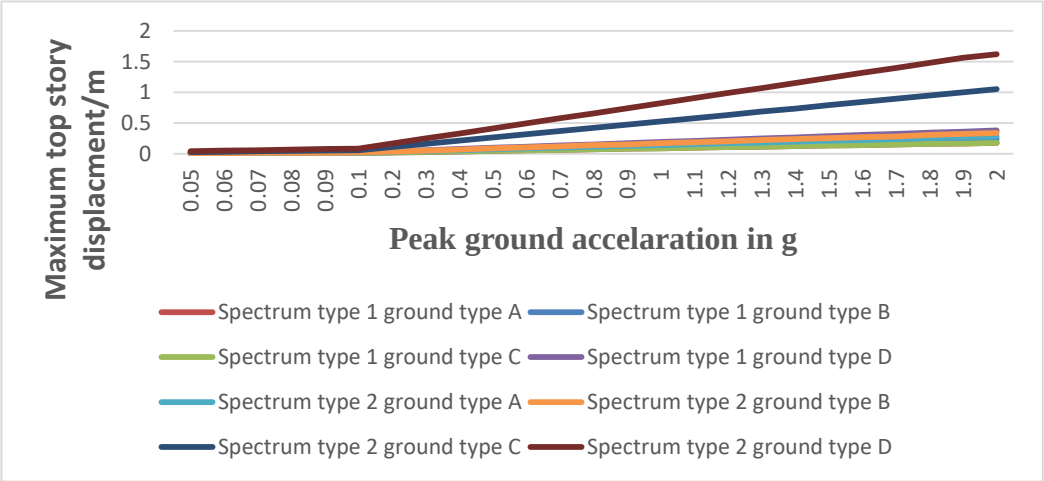


**Figure 4.7:Maximum top story displacements of the 12-story frame structures subjected to an earthquake motion.**

According to Tables 4.3-4.10, the vibration response of the top story is maximum under the action of both blasting wave and earth quake loads. From tables 4.3-4.10, as the number of bays increases maximum story displacements decreases for both blast loads and earth quake loads. In table 4.11 percentage increase of maximum story displacements of frame structures are obtained for equal blast loads and at the same stand of distance by changing story heights. The maximum percentage increases for all cases is 492.3070%.But from tables 4.12 and 4.13 maximum percentage increase of 1023.0769% is found when the story is constant and stand of distance changes, indicating that in blast loads stand of distance is the main factor than structure height. Table 4.12 indicates that the maximum story displacements increase with the increase of structure height for earth quake loads.

**Table 4.11:Percentage increase of maximum displacements of frame structure when an equivalent 3kg of TNT subsurface explosion at different stand of distance is subjected to 6-story and 12-story frame structure.**

| Number of Bay | Stand of distance(m) | Story | | Percentage increase of displacements in % |
|---|---|---|---|---|
| | | 6-story | 12-story | |
| (3x3) Bay | 4 | 0.0318 | 0.0761 | 139.3080 |
| | 7 | 0.0089 | 0.0187 | 110.1120 |
| | 10 | 0.0039 | 0.0081 | 107.6920 |
| (3x4) Bay | 4 | 0.0146 | 0.0617 | 322.6020 |
| | 7 | 0.003 | 0.0177 | 490.0000 |
| | 10 | 0.0013 | 0.0077 | 492.3070 |

**Table 4.12:Percentage increases of maximum displacements of 6-story frame structure when the structure is subjected to equivalent 3kg of TNT at different stand of distance.**

| Number of Bay | Stand of distance(m) | | Percentage increase of displacements in % |
|---|---|---|---|
| (3x3) Bay | 7 | 4 | 257.3033 |
| | 10 | 4 | 715.3846 |
| | 10 | 7 | 128.2051 |
| (3x4) Bay | 7 | 4 | 386.6666 |
| | 10 | 4 | 1023.0769 |
| | 10 | 7 | 130.7692 |

**Table 4.13:Percentage increases of maximum displacements of 12-story frame structure when the structure is subjected to equivalent 3kg of TNT at different stand of distance.**

| Number of Bay | Stand of distance(m) | | Percentage increase of displacements in % |
|---|---|---|---|
| (3x3) Bay | 7 | 4 | 306.9518 |
| | 10 | 4 | 839.5061 |
| | 10 | 7 | 130.8641 |
| (3x4) Bay | 7 | 4 | 248.5875 |
| | 10 | 4 | 701.2987 |
| | 10 | 7 | 129.8701 |

**Table 4.14:Percentage increase of maximum displacements of frame structure when an earthquake motion characterized by the elastic design spectrum (Type 1) of ES EN1998-1, 2015 scaled to 0.2gand 0.4g peak ground acceleration and for different ground types.**

| Number of bay | Peak ground acceleration in g | Ground types | 6-story | 12-story | Percentage increase in % |
|---|---|---|---|---|---|
| (3x3) bay | 0.2 | A | 0.0175 | 0.0383 | 118.4203 |
| | | B | 0.0236 | 0.0516 | 117.9698 |
| | | C | 0.0175 | 0.0385 | 119.0736 |
| | | D | 0.0378 | 0.0826 | 118.5185 |
| | 0.4 | A | 0.0344 | 0.0755 | 119.4767 |
| | | B | 0.0465 | 0.1020 | 119.3548 |
| | | C | 0.0351 | 0.0770 | 119.3732 |
| | | D | 0.0757 | 0.1652 | 118.2298 |
| (3X4) bay | 0.2 | A | 0.0083 | 0.0263 | 216.8674 |
| | | B | 0.0112 | 0.0355 | 216.9642 |
| | | C | 0.0122 | 0.0268 | 119.6721 |
| | | D | 0.0151 | 0.0563 | 272.8476 |
| | 0.4 | A | 0.0164 | 0.0522 | 218.2926 |
| | | B | 0.0221 | 0.0705 | 219.0045 |
| | | C | 0.0244 | 0.0535 | 119.2622 |
| | | D | 0.0303 | 0.1126 | 271.6171 |

### 4.5.3 Equivalent earth quake loads for the blast loads.

From tables 4.3-4.6 maximum floor displacements for (3x3) bay 6-story and 12-story was obtained and from tables 4.7-4.10 maximum top story displacements of

the (3x3) bay 6-story and 12-story frame structures subjected to an earthquake motion characterized by the elastic design spectrum (Type 1 and 2) of ES EN 1998-1, 2015 scaled to different peak ground acceleration and for different ground types was obtained. These two maximum responses are compared and equivalent earth quake loads for different spectrum type and ground types are established for blast loads produced by an equivalent 3 kg of TNT sub surface explosion at different stand of distances.

Table 4.15 and 4.16 shows equivalent earth quake loads for (3x3) bay 6-story and 12-story frame structure which can give comparable maximum displacements as blast loads of an equivalent 3kg of TNT sub surface explosion at different stand of distance.

**Table 4.15:Maximum comparable displacements of (3x3) bay 6-story frame structure produced by earth quake loads for blast loads of an equivalent 3kg of TNT sub surface explosion.**

| Stand of distance for blast loads of equivalent 3kg of TNT sub surface explosion | Maximum displacements/m | Spectrum type 1 | | | Spectrum type 2 | |
|---|---|---|---|---|---|---|
| | | Ground types | Peak ground acceleration in g | Maximum displacements/m | Peak ground acceleration in g | Maximum displacements/m |
| 4 | 0.0318 | A | 0.3 | 0.0263 | 0.2 | 0.0280 |
| | | | 0.4 | 0.0344 | 0.3 | 0.0420 |
| | | B | 0.2 | 0.0236 | 0.1 | 0.0169 |
| | | | 0.3 | 0.0355 | 0.2 | 0.0338 |
| | | C | 0.3 | 0.0263 | 0.1 | 0.0171 |
| | | | 0.4 | 0.0351 | 0.2 | 0.0342 |
| | | D | 0.1 | 0.0189 | 0.1 | 0.0200 |
| | | | 0.2 | 0.0378 | 0.2 | 0.0401 |
| 7 | 0.0089 | A | 0.1 | 0.0087 | 0.06 | 0.0084 |
| | | | 0.2 | 0.00175 | 0.07 | 0.0098 |
| | | B | 0.07 | 0.0082 | 0.05 | 0.0085 |

| | | | | | | |
|---|---|---|---|---|---|---|
| | | | 0.08 | 0.0094 | 0.06 | 0.0101 |
| | | C | 0.1 | 0.0087 | 0.05 | 0.0085 |
| | | | 0.2 | 0.0175 | 0.06 | 0.0101 |
| | | D | 0.05 | 0.0095 | 0.05 | 0.0100 |
| 10 | 0.0039 | A | 0.05 | 0.00438 | 0.05 | 0.0070 |
| | | B | 0.05 | 0.0059 | 0.05 | 0.0085 |
| | | C | 0.05 | 0.00439 | 0.05 | 0.0085 |
| | | D | 0.05 | 0.0095 | 0.05 | 0.0100 |

**Table 4.16:Maximum comparable displacements of (3x3) bay 12-story frame structure produced by earth quake loads for blast loads of an equivalent 3kg of TNT sub surface explosion.**

| Stand of distance for blast loads of equivalent 3kg of TNT sub surface explosion | Maximum displacement/m | Spectrum type 1 | | | Spectrum type 2 | |
|---|---|---|---|---|---|---|
| | | Ground types | Peak ground acceleration in g | Maximum displacements/m | Peak ground acceleration in g | Maximum displacements/m |
| 4 | 0.0761 | A | 0.2 | 0.0574 | 0.2 | 0.0610 |
| | | | 0.3 | 0.0766 | 0.3 | 0.0915 |
| | | B | 0.2 | 0.0516 | 0.1 | 0.0457 |
| | | | 0.3 | 0.0775 | 0.2 | 0.0914 |
| | | C | 0.3 | 0.0577 | 0.1 | 0.0525 |
| | | | 0.4 | 0.0770 | 0.2 | 0.1050 |
| | | D | 0.1 | 0.0413 | 0.09 | 0.0739 |
| | | | 0.2 | 0.0826 | 0.1 | 0.0821 |
| 7 | 0.0187 | A | 0.09 | 0.0172 | 0.06 | 0.0183 |
| | | | 0.1 | 0.0191 | 0.07 | 0.0214 |
| | | B | 0.07 | 0.0181 | 0.05 | 0.0229 |
| | | | 0.08 | 0.0207 | | |
| | | C | 0.09 | 0.0173 | 0.05 | 0.0263 |
| | | | 0.1 | 0.0192 | | |
| | | D | 0.05 | 0.0320 | 0.05 | 0.0411 |
| 10 | 0.0081 | A | 0.05 | 0.0096 | 0.05 | 0.0153 |
| | | B | 0.05 | 0.0129 | 0.05 | 0.0229 |
| | | C | 0.05 | 0.0096 | 0.05 | 0.0263 |
| | | D | 0.05 | 0.0207 | 0.05 | 0.0411 |

As shown in tables 4.15 and 4.16, when 6-story frame structure is analyzed for an earthquake motion characterized by the elastic design spectrum of ES EN1998-1, 2015 scaled to peak ground acceleration of 0.2g in ground types A,B,D and in spectrum type 1 and A,B,C in spectrum type 2,0.3g in ground type C and spectrum type 1,0.09g in ground type D and spectrum type 2 can give comparable maximum displacements as when the structure is analyzed for blast loads of an equivalent 3kg of TNT sub surface explosion at 4m stand of distance. For the blast loads at 7m stand of distance 0.08g in ground types A ,B,C and spectrum type 1 and peak ground accelerations of bellow 0.05g in the rest ground types and in both spectrum types can give comparable maximum displacements and for 10m stand of distance the displacements are insignificant. When 12-story frame structure is analyzed for an earthquake motion characterized by the elastic design spectrum of ES EN1998-1, 2015 scaled to peak ground acceleration of 0.2g in all ground types and spectrum type 1 and 0.1g in spectrum type 2 can give comparable maximum displacements as when the structure is analyzed for blast loads of an equivalent 3kg of TNT sub surface explosion at 4m stand of distance. For the blast loads at 7m stand of distance 0.09g in ground types A, B, C and spectrum type 1 and bellow 0.05g in all ground types and spectrum type 2 can give comparable maximum displacements and for 10m stand of distance the displacements are insignificant.

# CHAPTER 5 CONCLUSIONS AND RECCOMENDATIONS

## 5.1 Conclusions

In this thesis a selected bench mark building is analyzed for its response under sub surface explosion in sandy soil and under a serious of seismic ground motion characterized by the elastic design spectrum of ES EN 1998-1, 2015 scaled to different peak ground acceleration and 5% damping.

The variables used are explosion source distance for blast loads, different peak ground acceleration in different ground types for earth quake loads and, number of bays and height of the structure for both earth quake and blast loads.

By controlling one of the variables unchanged, the corresponding data of other variables are compared and analyzed to summarize variables influencing dynamic responses of RC frame structure for sub surface blast loads (mining blasting vibration) and earth quake loads to the surrounding RC frame structure. Equivalent earth quake loads are also established for blast loads of sub surface explosion considering maximum story displacements.

Based on the analysis carried out the following observation and conclusion can be drawn;

1. The vibration responses of top story RC frame structure is maximum under both blast loads and earth quake loads.

2. Maximum story displacements of RC frame structures decrease with the increase of number of bays for both blast loads and earth quake loads.

3. Maximum story drifts caused by blast loads of RC frame structure appears at the lower story.

4. The number of bays of the RC frame structure has greater impact on the story drift when the explosion source distance is small.

5. In blast loads stand of distance is the main influencing factor than story height.

6. For RC frame structure the maximum story displacement and maximum story drift are decreased with increase of distance from the explosion source, when the explosion source distance is large the dynamic response of the structure is very small even can be ignored. Therefore, safe distance should be determined for structure according to a situation in sub surface explosion or in blast mining area.

7. For RC frame structure the change rate of floor displacement is smaller when explosion distance is farther.

8. For spectrum type 1, maximum story displacement is attained when RC frame structure is analysed for an earthquake motion characterized by the elastic design spectrum (Type 1) of ES EN1998-1, 2015 scaled to different peak ground acceleration in ground type B than C. But for spectrum type 2 it is in contrary indicating that ground type B gives better dynamic responses when it is used in spectrum type 2 than 1.

9. The global responses of considered RC frame structures subjected to blast loads at nearer standoff distance and earth quake loads of 0.2g is almost comparable but at farther stands of distance the global responses of RC frame structure for the blast loads are insignificant.

## 5.2 Recommendations.

The following recommendations are suggested for further work;

1. Analysis of (RC) reinforced concrete structure for different amounts of sub surface explosions in different soil conditions.

2. Comparative global and local level analysis of different structure types like reinforced concrete structures and steel structures for different amounts of sub surface explosions to understand its effect on structures in detail.

3. Coupled analysis of RC reinforced concrete structure for sub surface explosions.

4. Generating general formula for (RC) reinforced concrete structure which relates seismic effects of blast loads to earth quake loads so that a structure can be

analyzed and designed for seismic effects of blast loads using procedures outlined in different codes to analyze and design a structure for earth quake loads.

## REFERENCES


1. M.Y.H. Bangash 1993, 'Shock Impact and Explosion Structural Analysis and Design', Springs UK.

2. T. Krauthammer 2008, "Modern Protective Structures", Taylor & Francis Group, LLC.

3. Manmohan Dass Goel and Vasant A. Matsagar 2014, 'Blast-Resistant Design of Structures', Article practice periodical on structural design and construction.

4. Ethiopian Building Code Standard 8, ES EN1998-1, 2015: 'Design of structures for earthquake resistance'.

5. Chopra 1995, 'Dynamics of Structures', Prentice-Hall, Inc. Englewood Cliffs, New Jersey.

6. Remennikov, AM 2003, 'A Review of Methods for Predicting Bomb Blast Effects on Buildings', Journal of Battlefield Technology, 6(3) pp 5-10. Published by Argos Press Pty Ltd.

7. Manassah, Jamal T. 2001, 'Elementary mathematical and computational tools for electrical and computer engineers using MATLAB'.

8. Kaoshan Dai 2009, 'Dynamic performance of transmission pole structures under blasting induced ground vibration', PhD theses, University of North Carolina at Charlotte.

9. SAP2000 Version Advanced 14.1.0 2009, 'Structural Analysis Program', Computers and Structures Inc.

10. Unified facilities criteria (UFC), UFC 3-340-02, 2008, 'structure to resist the effects of accidental explosions'. U.S. army corps of engineer's naval facilities engineering command (preparing activity) air force civil engineer support agency.

11. Abdulaziz Kassahun (2011), 'Blast loading and blast effects on RC frame buildings'.

12. Bibiana M. Luccionia, and Ricardo D. Ambrosinib, 2008, 'Evaluating the effect of underground explosions on structures'.

13. ASCE 2010, 'Design of Blast-Resistant Buildings in Petrochemical Facilities', American Society of Civil Engineers, Reston, Virginia.

14. Eve Roger 2015, 'Mines buried in dry and saturated soils', blast experiments, soil modelling and simulation.

15. Unified facilities criteria (UFC) 2009, 'design of buildings to resist progressive collapse' UFC 4-023-03. U.S. army corps of engineers (Preparing Activity) naval facilities engineering command air force civil engineer support agency.

16. FEMA 427 2003, 'Primer for design of commercial building to mitigate terrorist attacks', providing protection to people and building.

17. Yong Lu and Hong Hao 2002, 'Experimental Investigation of Structural Response to Generalized Ground Shock Excitations', Article in Experimental Mechanics.

18. Dan (Danesh) Nourzadeh,Jagmohan Humar and Abass Braimah 2017, 'Comparison of Response of Building Structures to Blast Loading and Seismic Excitations', 6th International Workshop on Performance, Protection & Strengthening of Structures under Extreme Loading, pp 11-12, Guangzhou (Canton), China

19. Mohammed s. Al- Ansari 2012, 'Building Response to blast and earthquake loading', International journal of civil engineering and technology (IJCIET) Volume 3, Issue 2, pp. 327-346.

20. ASCE standard ASCE/SEI 41-1 2014: American Society of Civil Engineers, 'seismic evaluation and retrofit of existing buildings'.

21. Carl Kisslinger, Emil J. Mafelcer. Jr., and Thomas V. McEvilly 1963, 'Seismic waves generated by chemical explosions', Saint Louis University, Institute of Technology.

22. W. W. Hays and T. R. Murphy 1969, 'Amplitude and frequency characteristics of elastic wave types generated by underground nuclear explosions', Environmental research corporation, Alexandria, Virginia.

23. Howard C. Rodean 1972, 'Explosion-produced ground motion: Technical summary with respect to seismic hazards', Lawrence Radiation Laboratory, University of California.

24. Sayed A. Dahy and Gaber H. Hassib 2010, 'Spectral Discrimination between Quarry Blasts and Micro earthquakes in Southern Egypt', Research Journal of Earth Sciences 2 (1): 01-07, 2010, Aswan Earthquake Research Centre, Aswan, Egypt.

25. J. R. Thoenen and S. L. Windes 1942, 'Seismic effects of quarry blasting', United States department of the interior bureau of mines.

26. Vitaly I. Khalturin, Tatyana G. Rautian, and Paul G. Richards 1998, 'The Seismic Signal Strength of Chemical Explosions', Bulletin of the Seismological Society of America, Vol. 88, No. 6, pp. 1511-1524.

27. T. Ngo, P. Mendis, A. Gupta & J. Ramsay 2007, 'Blast Loading and Blast Effects on Structures', The University of Melbourne, Australia.

28. J.M. Biggs 1964, “Introduction to Structural Dynamics”, McGraw-Hill, New York.

29. M.N. Fardis 2011, “Euro code (EC) 8: Seismic Design of Buildings”, Support to the implementation, harmonization and further development of the Euro codes, Lisbon.

30. M.N. Fardis & G. Tsionis 2011, “Specific rules for design and detailing of concrete buildings”, Design for DCM and DCH, Illustration of elements design, University of Patras (GR).

## APPENDIX A

For the horizontal components of the seismic action, the elastic response spectrum *Se*(*T*) is defined by the following expressions according to ES EN1998-1, 2015.

$$0 \le T \le T_B: \quad S_e(T) = a_g \cdot S \cdot \left[1 + \frac{T}{T_B} \cdot (\eta \cdot 2.5 - 1)\right]$$

$$T_B \le T \le T_C: \quad S_e(T) = a_g \cdot S \cdot \eta \cdot 2.5$$

$$T_C \le T \le T_D: \quad S_e(T) = a_g \cdot S \cdot \eta \cdot 2.5\left[\frac{T_C}{T}\right]$$

$$T_D \le T \le 4s: \quad S_e(T) = a_g \cdot S \cdot \eta \cdot 2.5\left[\frac{T_C T_D}{T^2}\right]$$

Where;

$S_e$(T) is the elastic response spectrum;

$T$ is the vibration period of a linear single-degree-of-freedom system;

$a_g$ is the design ground acceleration on type A ground

$T_B$ is the lower limit of the period of the constant spectral acceleration branch;

$T_C$ is the upper limit of the period of the constant spectral acceleration branch;

$T_D$ is the value defining the beginning of the constant displacement response range of the spectrum;

$S$ is the soil factor;

$\eta$ is the damping correction factor with a reference value of 1 for 5% viscous damping.

According to the above formulas and different parameters for different spectrum type and ground type Pseudo spectral accelerations are generated.

Values of the parameters describing the recommended Type 1 elastic response spectra are;

| Ground type | S | $T_B$(s) | $T_C$(s) | $T_D$(s) |
|---|---|---|---|---|
| A | 1 | 0.05 | 0.25 | 1.2 |
| B | 1.35 | 0.05 | 0.25 | 1.2 |
| C | 1.5 | 0.1 | 0.25 | 1.2 |
| D | 1.8 | 0.1 | 0.3 | 1.2 |

Values of the parameters describing the recommended Type 2 elastic response spectra are

| Ground type | S | $T_B$(s) | $T_C$(s) | $T_D$(s) |
|---|---|---|---|---|
| A | 1 | 0.15 | 0.4 | 2 |
| B | 1.2 | 0.15 | 0.5 | 2 |
| C | 1.15 | 0.2 | 0.6 | 2 |
| D | 1.35 | 0.2 | 0.8 | 2 |

According to the above explanation sample response spectrum curve generated in spectrum type 1, ground type A and peak ground acceleration of g which have to be used in sap 2000 software are shown below.

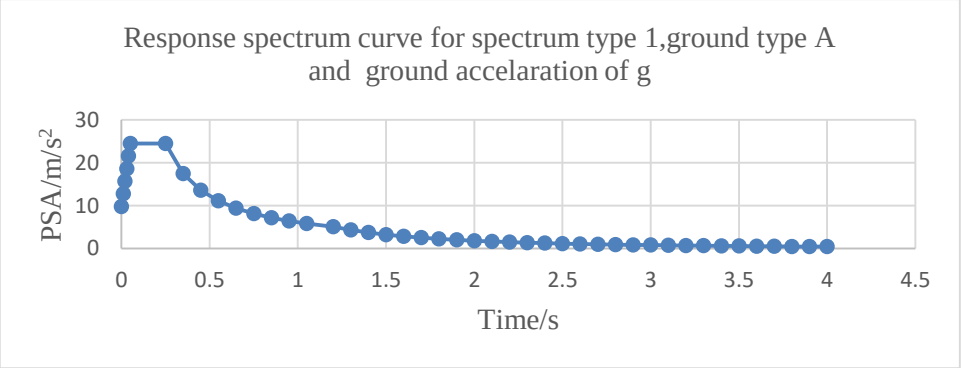


Appendix A figure-1: Sample elastic response spectrum curves.

Then this elastic response spectrum curve is reduced by behaviour factor to get design response spectrum curves.

For the horizontal components of the seismic action the design spectrum, $S_d(T)$, shall be defined by the following expressions:

$$0 \le T \le T_B: \quad S_d(T) = a_g \cdot S \cdot \left[\frac{2}{3} + \frac{T}{T_B} \cdot \left(\frac{2.5}{q} - \frac{2}{3}\right)\right]$$

$$T_B \le T \le T_C: \quad S_d(T) = a_g \cdot S \cdot \eta \cdot \frac{2.5}{q}$$

$$T_B \le T \le T_C: \quad S_d(T) = \begin{cases} = a_g \cdot S \cdot \frac{2.5}{q} \cdot \left[\frac{T_C}{T}\right] \\ \ge \beta \cdot a_g \end{cases}$$

$$T_D \le T: \quad S_d(T) = \begin{cases} = a_g \cdot S \cdot \frac{2.5}{q} \cdot \left[\frac{T_C \cdot T_D}{T^2}\right] \\ \ge \beta \cdot a_g \end{cases}$$

Therefore; according to the above formulas design response spectrum curve becomes;

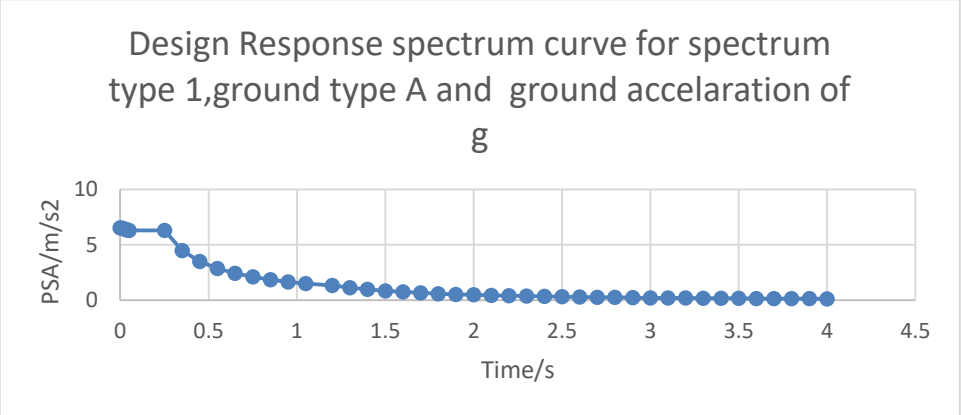


Appendix A figure-2: Sample design response spectrum curve.

## Appendix B

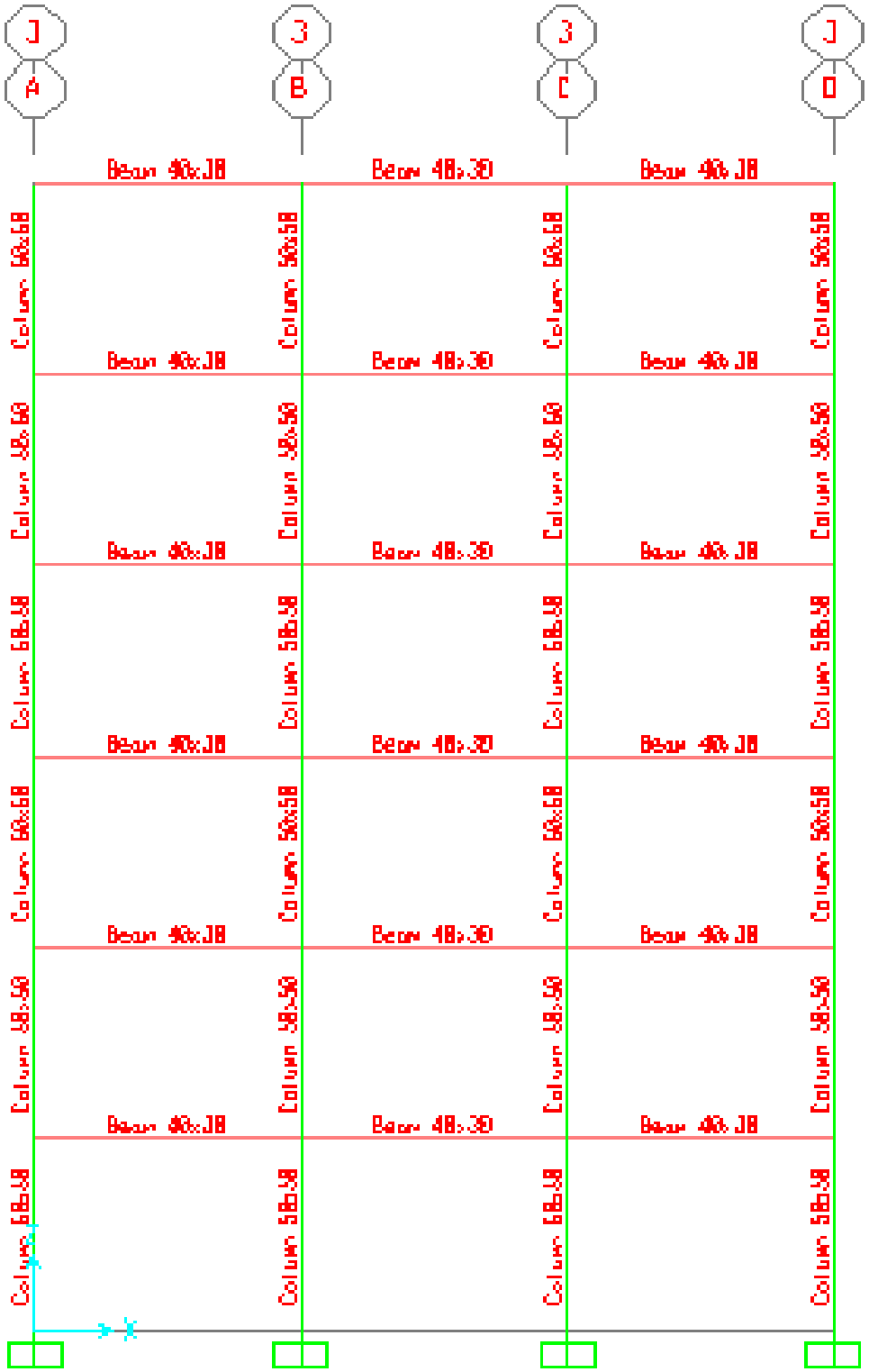


**Figure Appendix B- 1:** Sample design sections of 6-story models along axis-3

**Table Appendix B-1**: reinforcement requirements of typical beam for 6 story

| section | Section (mm) | Longitudinal Rebar | | Stirrup |
|---|---|---|---|---|
| | | Top | Bottom | |
| Typical beam | 40x30 | 6Φ16 | 3Φ16 | Φ8 C/C 100 |

**Table Appendix B-2**: reinforcement requirements of typical column for 6 story

| section | Longitudinal Rebar | Stirrup |
|---|---|---|
| Typical column | 12Φ16 | Φ8 C/C 150 |